Spectrum Splitting of Solar Radiation for Efficient Conversion via Photovoltaics

By

Behlol Nawaz

Reg#00000105473

Supervised by

Dr. Nadia Shahzad

US-Pakistan Center for Advanced Studies in Energy (USPCAS-E)

National University of Sciences and Technology (NUST)

Islamabad

January 2020

Spectrum Splitting of Solar Radiation for Efficient Conversion via Photovoltaics

By

Behlol Nawaz

Reg#00000105473

Session 2016-2018

Supervised by

Dr. Nadia Shahzad

A Thesis Submitted to the US-Pakistan Center for Advanced Studies in Energy in partial fulfillment of the requirements for the degree of

Master of Science in

Energy Systems Engineering

US-Pakistan Center for Advanced Studies in Energy (USPCAS-E)

National University of Sciences and Technology (NUST)

H-12, Islamabad 44000, Pakistan

Jan 2020

THESIS ACCEPTANCE CERTIFICATE

Certified that final copy of MS/MPhil thesis written by Mr. Behlol Nawaz, (Registration No. 00000105473), of U.S. – Pakistan Center for Advanced Studies in Energy has been vetted by the undersigned, found complete in all respects as per NUST Statues/Regulations, is within the similarity indices limit and is accepted as partial fulfillment for the award of MS/MPhil degree. It is further certified that necessary amendments as pointed out by GEC members of the scholar have also been incorporated in the said thesis.

Signature: _____

Name of Supervisor: Dr. Nadia Shahzad_____

Date: _____

Signature (HoD): _____

Date: _____

Signature (Dean/Principal): _____

Date: _____

CERTIFICATE

This is to certify that work in this thesis has been carried out by **Mr. Behlol Nawaz** and completed under my supervision in US-Pakistan Center for Advanced Studies in Energy (USPCAS-E), National University of Sciences and Technology, H-12, Islamabad, Pakistan.

Supervisor: _____

Dr. Nadia Shahzad
USPCAS-E
NUST, Islamabad

GEC member # 1: _____

Dr. Muhammad Rizwan Saleem
USPCAS-E
NUST, Islamabad

GEC member # 2: _____

Dr Bilal Sajid
USPCAS-E
NUST, Islamabad

GEC member # 3: _____

Mr. Rashid Wazir
SEECS
NUST, Islamabad

HoD - (Deptt.): _____

Dr. Naseem Iqbal
USPCAS-E
NUST, Islamabad

Principal/Dean: _____

Dr. Adeel Waqas
USPCAS-E
NUST, Islamabad

Dedication

I dedicate my thesis to my parents and sister, whose unconditional prayers and support have enabled me to come this far.

ACKNOWLEDGEMENTS

I would like to thank my advisors Dr. Nadia Shahzad and Dr. Muhammad Rizwan Saleem. This work would not have been possible without their continuous guidance, support and patience.

I would also like to acknowledge the contribution of Mr. Wisnu Ananda, who provided us with the external quantum efficiency (EQE) data for Silicon and Perovskite. Without it, the analysis of our designs would not have been possible.

ABSTRACT

Solar power has the raw potential to fulfill a considerable portion of global energy needs, while avoiding most of the negative side effects associated with conventional energy sources. Photovoltaics have many advantages among solar energy conversion technologies, but it has numerous challenges. One of them is the efficiency limit on single junction photovoltaics (Shockley-Queisser limit). An oft studied and used technique to work around this limit is to use multijunction PV cells. However, the commonly used stacked multijunctions are expensive and difficult to manufacture. Spectrum splitting techniques have the potential to minimize these issues and make multijunction photovoltaics more feasible.

The objective of this study is to investigate a specific method of spectrum splitting for achieving high efficiency photovoltaic cells. For this purpose, a methodology is devised for the design of a diffractive spectrum splitting system, which is focused on quickly designing a splitting system for any given combination of two laterally arranged PV cells. The design is carried out using physical optics as well as ray tracing and simulated in the optical design software Zemax Optic Studio.

A system is designed with a grating and lens combination that manages to split the 350nm to 1100nm band into two bands, 350 to 570 nm for Perovskite and 570 to 1100 nm for Silicon. Along with splitting, geometric concentration ratios of 3.27 and 5.46 are achieved for Silicon and Perovskite respectively. The photocurrent density resulting from this distribution of the spectrum is calculated by using it with experimental EQE data for Silicon and Perovskite and the AM 1.5 spectrum. It is found that the photocurrent from the combination of Si and Perovskite cells with the designed system is ~2.5 times the photocurrent without it.

Keywords: Photovoltaics, Lateral Multijunction, Spectrum Splitting, Diffractive, Optical Design.

LIST OF FIGURES

LIST OF TABLES

LIST OF CONFERENCE/JOURNAL PAPERS

Conference Paper

Behlol Nawaz, Muhammad Rizwan Saleem, Nadia Shahzad

Design of a Diffractive Spectrum Splitting System for Lateral Multijunction Photovoltaics using Ray Tracing

Presented at 6th IST-SRPC, 20th June 2019

Available online: 6th September 2019

Journal Paper

Behlol Nawaz, Muhammad Rizwan Saleem, Nadia Shahzad

Design and Analysis of a Diffractive Spectrum Splitting System for a Silicon-Perovskite Double Junction Solar Cell

(To be submitted)

LIST OF ABBREVIATIONS

PV	Photovoltaic
QE	Quantum Efficiency
EQE	External Quantum Efficiency
PCE	Power Conversion Efficiency
AM0	Air Mass 0
AM1.5	Air Mass 1.5
ASTM	American Society for Testing and Materials
FDTD	Finite Difference Time Domain
MJ	Multijunction
ALD	Atomic Layer Deposition
IPCC	Intergovernmental Panel on Climate Change
NREL	National Renewable Energy Laboratory
LSC	Luminescent Solar Concentrator
LSS	Luminescent Solar Splitter
CIGS	Copper Indium Gallium Selenide
DCG	Dichromated Gelatin
HOE	Holographic Optical Element
RCWA	Rigorous Coupled Wave Analysis
SJ	Single Junction
DJ	Double Junction
TJ	Triple Junction
SSBC	Spectrum Splitting Beam Concentration
IR	Infrared
UV	Ultraviolet
AR	Antireflective Coating
MEEP	MIT Electromagnetic Equation Propagator

YAG	Yttrium Aluminum Garnet
DE	Diffraction Efficiency
ASM	Angular Spectrum Method
VHL	Volume Holographic Lens
DNI	Direct Normal Irradiance
PMMA	Poly (methyl methacrylate)
KVDT	Kirchhoff Vector Diffraction Theory
HVDT	Hertz Vector Diffraction Theory

Table of Contents

CHAPTER 1: INTRODUCTION

1.1 BACKGROUND

Energy, in its various usable forms, has become a fundamental part of today's civilization and is necessary for what we now perceive as normal "day-to-day" life. It is a crucial part of all the spheres of activities in today's human societies, from growing and processing food, to transportation, trade, manufacturing, entertainment, research and innovation, almost no human activity today is possible without it.

Most of today's energy needs are met by the use of fossil fuels such as the various types of oil, coal and natural gas. These resources have been the backbone of human development as well as technological and industrial innovation, but their reserves are limited and expected to last a few more decades with the currently known reserves [1]. Furthermore, a more serious and immediate danger in the use of fossil fuels is their contribution to climate change [2]. Fossil fuels are primarily carbon-based compounds and release energy via combustion. The major gaseous emission due to their combustion is carbon dioxide, a well-known greenhouse gas which has been contributing to the increase in global temperatures. Other gases associated with the extraction and use of fossil fuels such as methane and nitrous oxide also contribute to global warming [2]. Besides warming, the release of CO_2, other gases and particulates from fossil fuels pollute the ecosystem causing problems such as increasing ocean acidity, creating smog and causing health problems [3]. Furthermore, the sourcing of fossil fuels as well as their processing are resource intensive activities, utilizing a lot of water and damaging the environment [4]. In short, the fossil fuel-based energy sources are contributing to climate change while also polluting the ecosystem in other ways.

The limited reserves and harmful side effects of fossil fuels means their usage is not sustainable. Sources which are not limited (i.e. renewable on human timescales) and are clean (the environmental impacts of their life-cycles are recoverable) are commonly known as alternative, renewable or sustainable energy sources. These include solar, wind, hydropower, nuclear, tidal, biofuel and geothermal among some others [5]. All these sources are the subject of on-going research and have their fair

share of challenges with respect to technology as well as limitations in their areas of applications [5]. These challenges affect their current economic viability, especially in competition with fossil fuels. Wind, tidal and geothermal sources are only available in certain locations whereas hydropower is feasible in very limited geographies. Biofuels require careful balancing to ensure that they are economically viable, renewable and clean at the same time [5]. Similarly, solar power technologies are costly and are also limited by the amount and type of solar insolation an area of earth receives. Though the geographical limitations in terms of solar insolation is a challenge, it is not even close to being as restricting as the other renewable sources. Furthermore, it might be surmountable with technology to some extent. Most renewable sources are intermittent, so the limitations of today's energy storage technologies are also a major hurdle to renewable energy sources [6].

All these problems are hinderances to the more widespread use of sustainable sources and are therefore, being actively researched worldwide. The focus of this thesis is on the increase in efficiency of a specific variant of solar power technology. Solar was chosen due to its global availability, enormous raw potential and other characteristics, which will be discussed ahead.

1.1.1 Solar Energy and Solar Energy Technologies

Solar energy is the energy emitted by the sun. Like other stars, this is the result of fusion of atomic nuclei. In case of the class of stars to which our sun belongs, the fusion is between hydrogen nuclei which forms helium. The resulting energy is emitted in the form of electromagnetic radiation with components in most of the electromagnetic spectrum, below 300nm all the way up to 3000nm in wavelength [7]. But most of the energy output is in the infrared-visible-ultraviolet region. The radiation from the sun measured above the Earth's atmosphere can be reasonably approximated by black-body radiation at a temperature of approximately 5800 K [8]. The large distance between the Earth and sun as well as this solid angle implies that the direct solar irradiance can be considered collimated for most applications.

Travelling through the earth's atmosphere, the different wavelengths of the solar radiation are absorbed and scattered by the various components of the atmosphere such as oxygen, carbon dioxide, nitrous oxide, methane, ozone, water vapour etc. Below the

atmosphere, the solar irradiance (Global) usually peaks around a 1000W/m^2 [9], for specific conditions that are normally used for testing (discussed ahead).

Standard or reference spectra of solar radiation are defined according to the air masses they encounter, which primarily consider the length the radiation travels in the atmosphere. Air mass (or AM) defines the volume of air, considering its temperature and vapour content [9]. AM0 spectrum is the spectrum of solar radiation in space, above the atmosphere. This is usually considered for space based solar power applications, e.g. powering satellites. The spectrum of solar radiation when the sun appears directly above a point on earth is the AM1 spectrum. The spectrum more commonly used in testing and evaluation of terrestrial (i.e. earth based) solar power systems is the AM1.5, which means the solar radiation encounters 1.5 times the height of atmosphere and corresponds to a solar zenith angle of 48.19 degrees. The tabulated values of all these spectra are available on the National Renewable Energy Laboratory's (NREL) website [7].

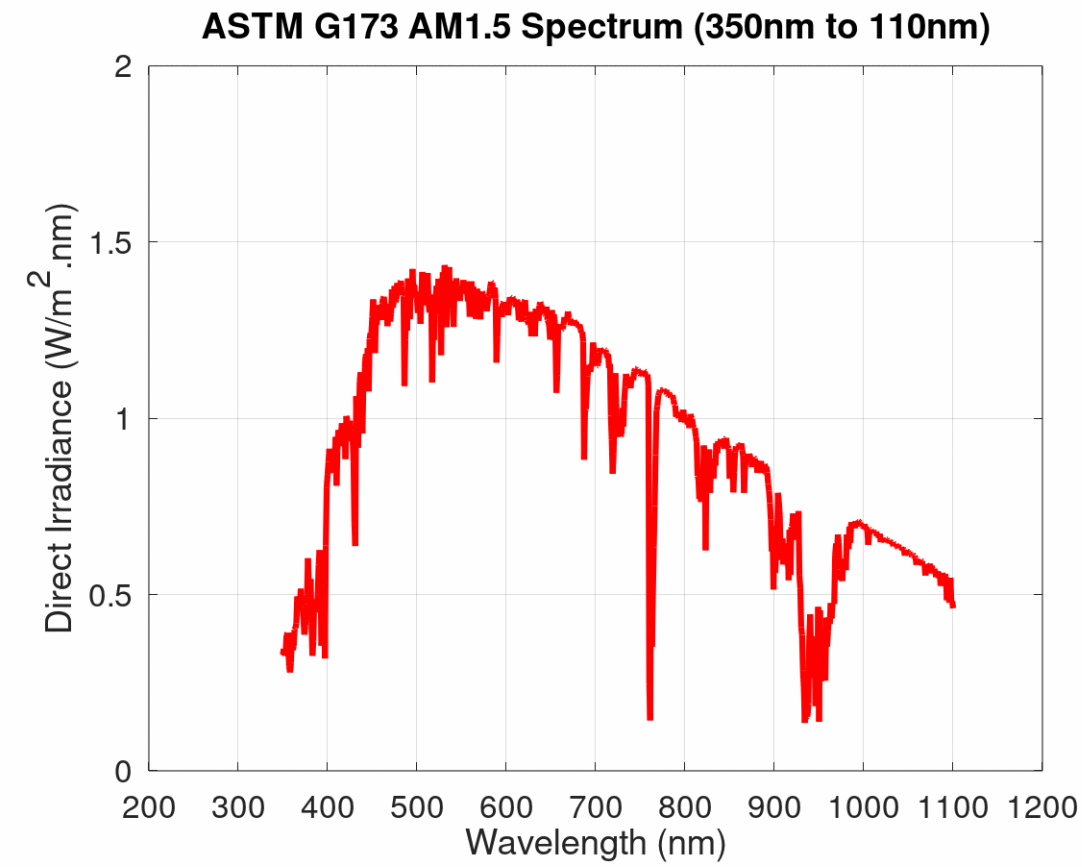

Figure 1: AM 1.5 Solar Spectrum

The irradiated power is usually classified into Direct Irradiance (which is the solar radiation that strikes the surface of the earth directly) and Diffused Irradiance (which is scattered by the atmosphere before reaching the surface). The combination of these two is known as the Global Irradiance. The ratio of Direct to Diffused in Global as well as the total global irradiance varies with atmospheric and environmental conditions. The 1000W/m^2 figure mentioned before is the Global irradiance for AM1.5 under a clear sky. The behavior of the solar spectrum incident on a solar cell directly affects its performance, as will be discussed ahead.

1.1.1.1 Common methods of utilizing solar energy

Numerous methods for converting solar energy incident on the Earth's surface into useful forms have been devised [5]. Some have already become commercial technologies, though almost all of them are still the subject of on-going research, to make them more feasible and economical on larger scales. Solar power technologies can be broadly divided into three categories. The most popular and widely known is the photovoltaic technology, which converts solar energy directly into electricity [5]. The second category is solar thermal, which consists of systems that utilize the heat of solar radiation [5]. This could be for direct heating or steam generation for electricity. Technologies of this category are also in use on a commercial basis. The third category is solar chemical, which generates fuels via chemical reactions that use solar energy [10].

1.1.1.2 Photovoltaics (Solar Electric)

In photovoltaic cells, the energy of the incoming photons of solar radiation are directly converted into electrical energy through the photovoltaic effect [5]. The electrical energy can then be stored in batteries or directly operate an electrical load. Solar cells use semiconductor materials that can undergo the photovoltaic process efficiently. Some materials used for photovoltaic cells include Silicon, Gallium Arsenide, Cadmium Sulfide, Copper Indium Gallium Selenide, Perovskites among others. Each material is efficient in conversion over a specific band of wavelengths.

One of the greatest advantages of photovoltaics compared to the other methods is the ease of deployment. The product of solar cells is electricity itself, one of the most common form of energy used by humans for various tasks. So there is no need for further electricity generation systems that have to be used with other solar

technologies. It can be scaled to work for a single room as well as an entire city. A major downside to photovoltaics is its intermittent nature. It must be stored for continuous supply of electricity. In addition to its own cost and efficiency issues, photovoltaic systems are often bottlenecked by the performance, cost and reliability of battery technologies.

1.1.1.3 Solar Thermal

Solar thermal technologies convert the radiation from the sun into heat energy [5]. This is often achieved by concentrating the solar radiation, which raises the temperature at the point of concentration. This could be for heating a working medium for generation of electricity (e.g. turning water into steam to turn a turbine or molten salt power plants) or using the heat energy directly for heating buildings, desalinating water etc.

Solar thermal technologies often need concentrators in the form of mirrors or lenses and can utilize a larger part of the incoming spectrum for raising temperature than a photovoltaic cell utilizing a single material. However, they typically require large specialized power plants to generate a significant amount of power as there must be concentrators as well as the systems that convert the heat into electricity. Also, solar thermal generation systems are not as easy to scale as photovoltaics. Furthermore, the generated power is still intermittent and needs to be stored or complemented by other sources.

1.1.1.4 Solar Chemical

Solar chemical methods use solar energy to carry out chemical reactions that generate fuels [10]. One widely studied solar chemical technique is the photocatalytic splitting of water into hydrogen and oxygen. Hydrogen can then be used as a fuel in fuel cells or even internal combustion engines. Another attractive solar chemical process is the reduction of carbon dioxide, which can be used to convert carbon dioxide into organic molecules and fuels. This can not only help in generation of solar energy-based fuels as alternatives to fossil fuels, but also in carbon fixation. The fuels can be used to generate electricity and can usually be stored en masse using existing methods for fossil fuels (excluding the case of hydrogen). However solar chemical conversion processes are currently highly inefficient and the usage technologies (fuel cells or engines) as well as storage technologies for hydrogen are not ready for widespread use.

The focus of this thesis is on a particular type of photovoltaic technology.

1.1.2 Overview of Photovoltaics

As already mentioned, photovoltaics is the class of solar power conversion technologies that convert the sun's energy directly into electricity. The following subsections give a brief overview of how photovoltaic cells generally work and their current challenges.

1.1.2.1 Technology – How it works

A photovoltaic cell usually consists of a semiconductor p-n junction. Semiconductor materials have valence electrons that are easier to mobilize than insulators, but not completely free like metals. A p-n junction is the intersection of two "doped" types of semiconductors, one with free electrons (n-type material) and the other with places that electrons can occupy called holes (p-type material). The p and n type materials can be of the same material or different ones, called homojunction and heterojunction respectively. While there is more of each carrier on a specific side of the junction, overall each material type is charge neutral, i.e. there is no excess charge. The excess electrons and holes on either side of the intersection diffuse to the other side and combine, creating a negatively charged region on the p-type side and positively charged region near the junction on the n-type. The mobile charge carriers (electrons and holes) are depleted in this region on both sides of the junction (as both electrons and holes are now combined). It is therefore called the "depletion region" and it has an electric field directed from the n-type depletion region to the p-type depletion region due to the carriers that had diffused there earlier [8].

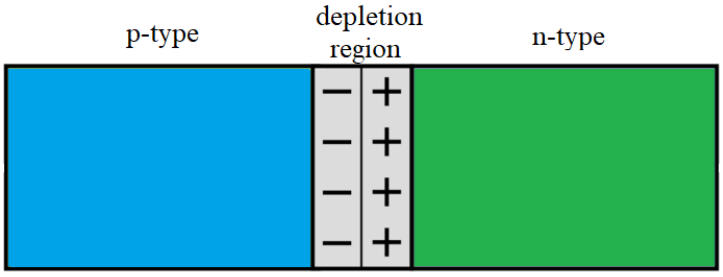

Figure 2: PN Junction with depletion region

When photons of solar energy above a certain threshold called the "bandgap" of the material strike the semiconductor material, they eject an electron from the valence band to the conduction band, creating and "electron-hole" pair (sometimes called

exciton). If the electron-hole pair reaches the junction before recombining, the electric field there would separate the electron-hole pair and the electron would be forced through the external circuit in order to recombine with the hole. Therefore, working on the electrical load in the external circuit.

1.1.2.2 Concept of bandgap and limitation on PV efficiency

As mentioned above, the energy of the photon of incoming radiation has to be more than the bandgap of the semiconductor material. Bandgap energy, E_g is the energy difference between the valence band of the material and the conduction band (the band of energy at which the electron is outside the influence of its atom) [8].

If the energy of the photon is less than E_g, it will not excite the electron into the conduction band, therefore not creating an electron-hole pair. In other words, the energy of all such radiation is wasted. On the other hand, if the energy of the photon is a lot higher than the bandgap, most of the excess energy of the photon is wasted and only one electron hole pair is generated (usually).

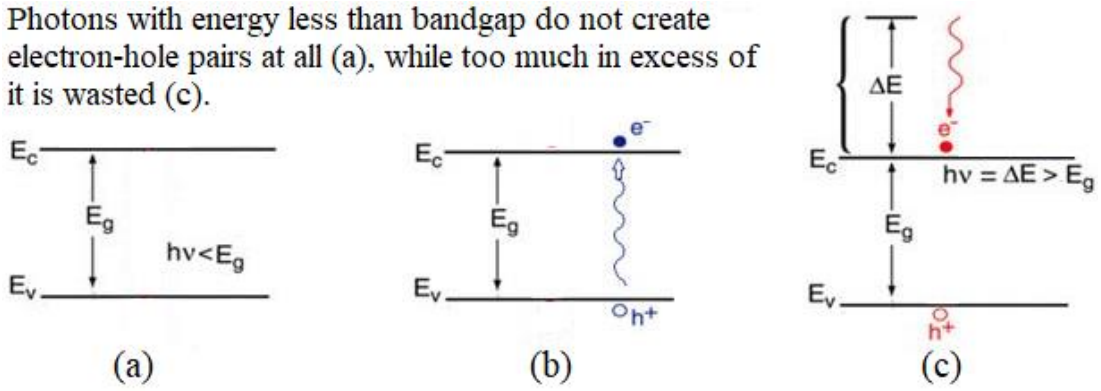

Figure 3: Photon Energy, bandgap and electron-hole pair generation

As the energy of a photon depends on its associated wavelength ($E = h \cdot f$), a specific material that has a specific bandgap can efficiently convert a limited number of wavelengths. Some wavelengths aren't converted into electrical energy at all, while the excess energy of higher energy wavelengths is wasted as thermal energy.

1.1.2.3 Need for multijunction cells

As a single junction of given material(s) can only convert a specific range of wavelengths efficiently, there is a limit on the efficiency that can be achieved by a single junction PV cell. This limit (known as the Shockley-Queisser limit) was first published in 1961, considering other effects that limit the efficiency as well. For 1.1

eV bandgap device (Silicon) working under solar radiation approximated with black body radiation at 6000K, it was found to be 30% [11]. According to more recent studies using the now standard ASTM G-173 1.5G solar spectrum, the maximum efficiency possible could be up to 33.7 % for an ideal 1.34 eV bandgap device[12]. Several methods have been studied to circumvent this limit. One is to have multiple junctions of different bandgaps, each converting bands of wavelengths that it can convert efficiently. There are two major configurations in which multijunction (MJ) cells have been studied [13].

1.1.2.4 Stacked multijunction cells

Vertically stacked multijunction cells (also called monolithic MJs) consist of different junctions, cascaded one on top of the other [13]. Certain wavelengths (usually shorter ones) of the sunlight coming from above are absorbed by the topmost layer while the remaining continue onwards to the next p-n junction. It absorbs its relevant wavelength bands and so on. The splitting of incoming sunlight into bands for each junction is achieved by the fact that wavelengths with energy less than the bandgap move on through the material to the next layer. To avoid unwanted interactions between adjacent layers of p-n junctions, tunnel junctions must be layered in between them.

Most of the highest performing, experimental MJ cells today are these stacked MJ cells under concentrated sunlight [14].

1.1.2.5 Lateral multijunction cells

The second approach to multijunction cells is to split the incoming spectrum of solar radiation into different bands before they reach the PV cell junctions. Only the required bands of wavelengths reach their respective junctions. PV material layers are often arranged “laterally” with this approach, though different geometries have been studied that use the same mechanism, where the light is split via optical manipulation before it reaches the p-n junctions.

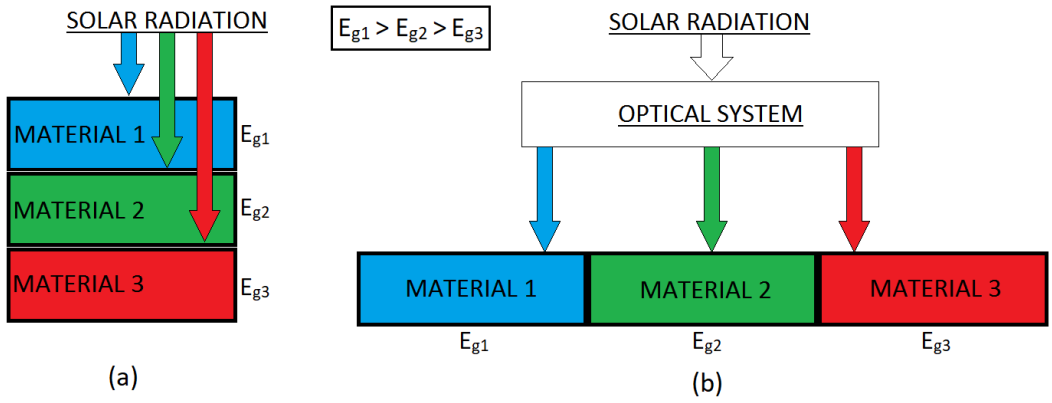

Figure 4: Stacked vs Lateral Multijunctions

Multijunction cells that use such spectrum splitting techniques have some potential advantages over the stacked multijunction cells. The crystal structures of the different layers of materials in a stacked multijunction need to be compatible. They require "lattice matching" to be reliably fabricated one on top of the other. This limits the combinations of photovoltaic materials that can be used to those with similar crystal structures, even though the combination of bandgaps may not perfectly complement each other. Furthermore, it requires costly manufacturing techniques like Atomic Layer Deposition (ALD), increasing its cost. Lateral multijunction cells are not affected by either of these constraints [13].

The various p-n junctions layered over each other in the monolithic multijunctions need to be separated from each other via tunnel junctions, to avoid the interaction of p and n regions of different layers from interacting with each other. The tunnel junctions must provide a low resistance path that is transparent to the incoming solar radiation so as not to affect the light passing on to the lower layers. This is another extra need in the stacked multijunctions that is avoided in lateral multijunction cells [13].

Another advantage is the fact that each cell experiences only the radiation it can convert efficiently. There are no chances of the other wavelengths being absorbed for increase in temperature. This decreases the temperature that the material of each junction must endure over its operational life. As a result, the degradation rate is slower, and the operational life of the cell is increased [15].

However, the major challenge for such multijunction cells with separate spectrum splitting is to design spectrum splitting systems that can divide the incoming solar radiation into bands of wavelengths and direct the required bands onto the

corresponding PV absorbers in the cells. This must be done accurately and efficiently to ensure the gains in overall efficiency of the cell.

1.2 Scope and Thesis Outline

This thesis is focused on designing a spectrum splitting system for lateral multijunction solar cells. The target is to design a basic splitting setup, with a simple methodology, while trying to use optical elements that are as close to off-the-shelf components as possible. The purpose of such a setup would be to easily study the interaction of design parameters of the system with its performance. Another aim is to lay down a design methodology which could be easily used to come up with such a setup for any combination of a lateral, two-junction cell, thereby allowing a quick way to verify the performances of different combinations of lateral multijunction cells.

This text introduces solar power and provides context to the lateral multijunction solar cells. The recent research into the categories of techniques that are often utilized for spectrum splitting are explored in the chapter on literature review. The methods are classified according to the optical methods used and the chosen class of splitting technique is discussed in further detail.

This is followed by the discussion of the design methodology, where the underlying theory of the major options from the chosen technique are discussed. Then using the discussed theory, the design methodology is proposed and utilized to come up with a design for a Silicon-Perovskite lateral dual junction.

The penultimate chapter details the results for the different configurations possible with the design and why a particular configuration is more desirable than other. It also explains the method for analysis of the obtained results and the consequent analysis. The results and analyses are then discussed in the backdrop of the earlier literature review. The concluding chapter discusses the takeaway points for the study and suggests possible improvements to the study as well as the possibilities for extending this work in the future.

1.3 Summary

This introductory chapter started off by providing the context of global energy challenges and the need for alternative energy source. This was followed by a brief overview of the various options in solar power technologies along with a discussion of

the solar spectrum. The basic technology of photovoltaics was discussed and a major reason for the efficiency limit of the simple, most popular variant of photovoltaics (single junction) was explained. This led to a discussion about how multijunction cells averted the limit. A comparison of the two major categories of multijunction cells (stacked and lateral) was made and their current challenges were explored. The choice to pursue lateral multijunctions was made based on the background and comparisons. The last section laid down the scope of this thesis and its outline.

1.4 REFERENCES

[1] N. Abas, A. Kalair and N. Khan "Review of fossil fuels and future energy technologies," *Futures*, vol. 69, pp. 31-49, 2015.

[2] T. F. Stocker, D. Qin, G.-K. Plattner, M. Tignor, S.K. Allen, J. Boschung, A. Nauels, Y. Xia, V. Bex and P.M. Midgley (eds.) *"Climate Change 2013: The Physical Science Basis. Contribution of Working Group I to the Fifth Assessment Report of the Intergovernmental Panel on Climate Change,"* IPCC/Cambridge University Press, 2013, Cambridge, United Kingdom.

[3] F. P. Perera, "Multiple Threats to Child Health from Fossil Fuel Combustion: Impacts of Air Pollution and Climate Change," *Environmental Health Perspectives*, vol. 125, no. 2, pp. 141-148, 2017.

[4] D. J. Rodriguez, A. Delgado, P. DeLaquil, and A. Sohns, "Thirsty energy," *Water Papers*, 2013, World Bank, Washington DC.

[5] O. Ellabban, Haitham Abu-Rubb, Frede Blaabjerg, "Renewable energy resources: Current status, future prospects and their enabling technology," *Renewable and Sustainable Energy Reviews*, vol. 39, pp. 748-764, November 2014.

[6] S. O. Amrouche, D.Rekioua, T.Rekioua, S.Bacha, "Overview of energy storage in renewable energy systems," *International Journal of Hydrogen Energy*, vol. 41, no. 45, pp. 20914-20927, Dec. 2016.

[7] ASTM Subcommittee G173-03, "*Standard Tables for Reference Solar Spectral Irradiances: Direct Normal and Hemispherical on 37° Tilted Surface"*, ASTM International, West Conshohocken, PA, 2012.

[8] P. Würfel, *Physics of solar cells: from principles to new concepts*. Weinheim, Wiley-VCH, 2005.

[9] A. Gombert and A. Luque, "Photonics in photovoltaic systems," *Physica Status Solili (A)*, vol. 205, no. 12, pp. 2757–2765, Dec. 2008.

[10] N. Armaroli and V. Balzani, "Solar Electricity and Solar Fuels: Status and Perspectives in the Context of the Energy Transition," *Chem. Eur. J.*, vol 22, no. 1, pp. 32-57, January 2016.

[11] W. Shockley and H. J. Queisser, "Detailed Balance Limit of Efficiency of p-n Junction Solar Cells," *Journal of Applied Physics*, vol. 32, no. 3, pp. 510–519, Mar. 1961.

[12] S. Rühle, “Tabulated values of the Shockley–Queisser limit for single junction solar cells,” *Solar Energy*, vol. 130, pp. 139–147, Jun. 2016.

[13] A. G. Imenes and D. R. Mills, “Spectral beam splitting technology for increased conversion efficiency in solar concentrating systems: a review,” *Solar Energy Materials and Solar Cells*, vol. 84, no. 1–4, pp. 19–69, Oct. 2004.

[14] M. A. Green *et al.*, “Solar cell efficiency tables (Version 53),” *Progress in Photovoltaics*, vol. 27, no. 1, pp. 3–12, Jan. 2019.

[15] C. Michel, J. Loicq, T. Thibert, and S. Habraken, “Optical study of a spectrum splitting solar concentrator based on a combination of a diffraction grating and a Fresnel lens,” in *AIP Conf. Proc. 1679*, Aix-les-Bains, France, 2015, pp. 070002-1-070002–7.

CHAPTER 2: LITERATURE REVIEW

2.1 OVERVIEW OF SPECTRUM SPLITTING METHODS

The idea of spectrum splitting for solar energy is decades old, having been discussed at least as early as 1955 [1]. Since then many methods, techniques and geometries have been studied.

The classification of spectrum splitting multijunction cells can vary by the author and the perspective taken up for a specific study. Generally, they could be categorized by the optical phenomena used for splitting. Common among these are luminescence, selective reflection/transmission, refraction and diffraction. Many designs have also used combinations of these techniques as well.

2.1.1 Luminescent Splitting and Concentrating Systems

The use of luminescent solar concentrators (LSC) was discussed by Weber and Lambe in 1976[2]. Gotzberger and Greubel introduced the idea of splitting and concentration independently in the following year [3]. The basic idea of this method is to embed a fluorescent dye in a transparent, optical waveguide plate. The dye absorbs sunlight and re-emits in longer wavelengths that are characteristic of the material. About 75-80% of this light is usually trapped in a transparent plate (of refractive index n =1.5) via total internal reflection [4] and guided towards the edge, which has the solar cells. Ideally, the energy of these emitted photons is a little greater than the band gap of the attached PV cells, to ensure a high conversion efficiency. Multiple layers of fluorescent materials that absorb specific wavelengths and allow others to pass through can then be used to split the incoming spectrum. Each such waveguide with fluorescent material can be used to successively absorb different bands of sunlight and emit their characteristic wavelengths towards their solar cell. The underlying physical mechanism behind fluorescent materials for such applications is reviewed in further detail in [4].

There are a number of advantages that make luminescent solar concentrators/splitters attractive. They can split and concentrate direct as well as diffused sunlight. They can be easily integrated into building facades and replace windows to generate electricity, with no aesthetic cost. They are also extensible to larger numbers of band gaps without

the need for a redesign of the entire system [5]. They do not require any expensive tracking system and reduce the area of solar cell material, as the light is collected by the dye doped plastic or glass instead. As transparent plastic or glass has a lower cost than a solar cell of comparable area, the cost per unit of power produced could be lower as compared to the same area of a photovoltaic material.

However, luminescent splitting and concentrating systems usually have very low power conversion efficiencies due to many loss mechanisms. The losses are due to reflected and transmitted light, non-ideal absorption quantum efficiency, overlap between absorption and emission bands which cause re-absorption, loss of absorbed solar energy via thermalization etc [6]. More seriously, fluorescent materials are prone to degradation over time and have short lives under solar radiation and heat. This hampers their practical utility at the moment.

Research into LSCs has mostly been focused on the engineering of materials to reduce the losses as well as degradation rates of the fluorescent dyes. Meinardi et al [7] studied the use of emissive silicon quantum dots, choosing Silicon due to its non-toxic nature along with low-cost and abundance. The dependence of absorption/emission on the sizes of quantum dots was used to tune the absorption/emission spectra, engineering a "Stokes shift" (i.e. difference between the maxima of the absorption and emission spectra). The study reported a Stokes shift of ~400meV for the 4.3nm diameter Si QDs, which the authors assert is a lot larger than the few tens of meV in core-only, metal chalcogenide QDs and comparable to reabsorption free QDs. Optical waveguides of 144cm^2 area and thickness of 0.26cm were fabricated by integrating these Silicon QDs into an acrylic matrix. An optical efficiency of η=2.85% was achieved for the transparent waveguide. Flexible waveguides were also tested as LSCs and it was observed that device curvature did not have any significant effect on its performance as an LSC. This observation combined with the fact that up to 70% transmittance was recorded across the visible spectrum makes it a good candidate for integration into buildings. According to Monte Carlo simulations, optimized silicon quantum dot LSCs can achieve optical efficiencies (η) up to $\eta > 5\%$ for 1m^2 devices with higher thicknesses. Although splitting wasn't part of the study, these properties would make the reported design useful for splitting with multiple layers and tunability.

Another recent study [8] reported LSCs based on chalcogenide QDs, for splitting and concentration. Two types of QDs were used, $CuInSe_2$ (narrow bandgap) and Mn_{2+} doped $Cd_xZn_{1-x}S$ (wider bandgap) for two different layers. The QDs were ~7.9nm and ~3.7nm in diameter respectively. This study also focused on tuning the spectra of the QDs. The resultant 232cm^2 device had an optical quantum efficiency of 6.4% and a power conversion efficiency (PCE) of 3.1% (top and bottom layers exhibited PCEs of 1.3% and 1.8% respectively). It was observed that the increase in efficiency due to the multijunctions (as compared to single-layer devices) increased with increasing LSC size and the authors predicted it could reach more than 120% with window sizes of area more than 50x50 cm^2.

One of the major reasons for losses in luminescent solar concentrators is the reabsorption of emitted light in the waveguide. The geometric dimensions of an LSC dictate the extent to which reabsorption affects the performance of an LSC, [9] i.e. the aspect ratio. For luminescent concentrators, by definition, it is the concentration factor. This means that it is difficult to simultaneously maximized concentration and spectrum splitting and a compromise is needed to increase the actual efficiency of the device. A study by Fischer and Biddle [5] investigated the use of luminescence for splitting (i.e. a luminescent solar splitter), while considering concentration as a by-product in the design (most designs focus on concentration while splitting is considered a secondary target). It was observed that the optical quantum efficiency as well as power efficiency of a cylindrical LSS (luminescent solar splitting) can be much higher for a purpose built LSS, rather than those realized in typical LSCs. They identified a conceptual design with quantum efficiency (QE) of up to 95%, with concentration ratios between 2x and 10x. According to their calculations, the PCE could exceed 30% with four junctions, using existing PV materials. However, this comes with the obvious sacrifice of optical concentration. According to them, advances in aligned anisotropic luminescence might be able to circumvent the need for compromise between LSS efficiency and net the concentration ratio. However, anisotropic luminescence needs further study before it can be applied for the said purpose [5].

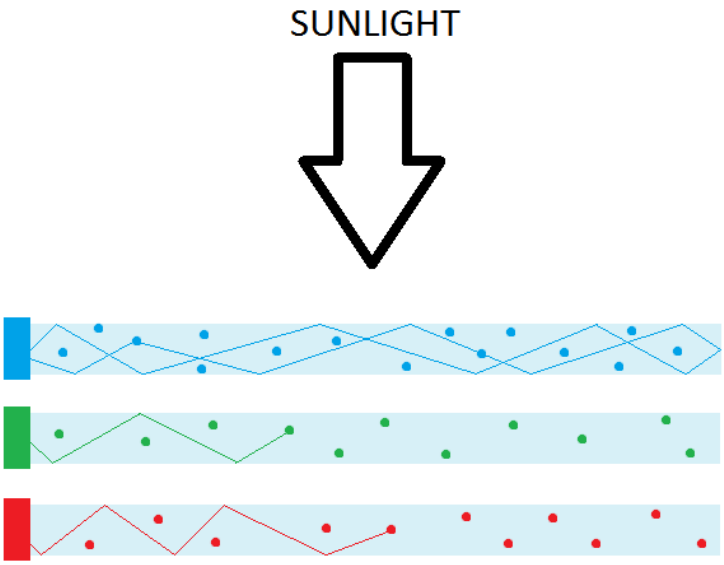

Figure 5: Luminescent Solar Splitter/Concentrator

2.1.2 Refractive Spectrum Splitting

Light waves travelling between different media can change direction in accordance with Fermat's principle and Snell's law, a behaviour known as refraction. The extent to which the direction changes depends on the refractive index a specific wavelength experiences in the given material. As a result, polychromatic light can disperse into its constituent wavelengths (commonly observed in prisms) and the extent of separation depends on how much the refractive index varies between wavelengths (quantified by Abbe number) for the material. In refractive spectrum splitting, this effect is utilized by designing the surface of a transparent material to manipulate the effect of dispersion for simultaneous splitting and concentration of solar radiation.

A design methodology devised by Stefancich et. al. utilizes refraction by combining an array of small prisms [10]. Every prism splits the incoming light into different wavelength bands. The design of the prisms and their overall arrangement ensures that the focus of each prism for a specific wavelength overlaps with the foci of all the prisms for that wavelength. The resulting beam is therefore concentrated and spectrally separated. In terms of geometry, the important design parameters are the angle of intersection of incoming light with the prism, the apex angle of the prism, the angle of the PV receiver with respect to the optical axis and the distance of the receiver from the apex of the prism. Each design parameter needs to be set with careful consideration as maximizing one desired characteristic (such as separation) leads to adverse effects in another (e.g. sensitivity to tracking errors and losses). The authors also noted that

the Abbe number of the material for the optical element needs to be a balance. A high dispersion material would result in better separation, but the higher refractive indices would also mean higher reflection losses. The manufacturing cost is also identified as an important consideration in the choice of material.

Working along the lines of this methodology, Maragliano et al designed a splitting and concentrating system which added curvature to the shape of the optical element in the dimension in which the prism was extruded [11]. This resulted in a more compact device and higher concentration, as the focus of this design is a point, rather than a line as in the notional design presented with the methodology in the paper by Stefancich et al. The final device which was manufactured from polycarbonate via injection moulding, had an approximate area of the device is 7x3 cm^2, with an average thickness of 2 mm. Thirty (30) trapezoidal prisms were used in this volume. The design was simulated with TracePro using an incident beam. The receiver was placed at a distance of 36 cm along the axis of the optical element and 23 cm below it. The optical transmissivity achieved was above 90% in the range of 400-800 nm. The authors estimate that the designed system would achieve an approximate efficiency of 30% with 1st generation wafer-based cells (Germanium, Silicon, GaAsP). In a subsequent study, [12] the device was tested with a pair of Copper Indium Gallium Selenide (CIGS) cells with the ratio of Indium to Gallium varied to achieve different bandgaps. The power conversion efficiency (PCE) increases from 13.6% to 15.1% (IoBB of 8.28%). The low increase was attributed to the unoptimized bandgaps of the two PV cells. The authors estimated that a slightly more optimized combination of three cells could reach a PCE of 26.5% with the designed system.

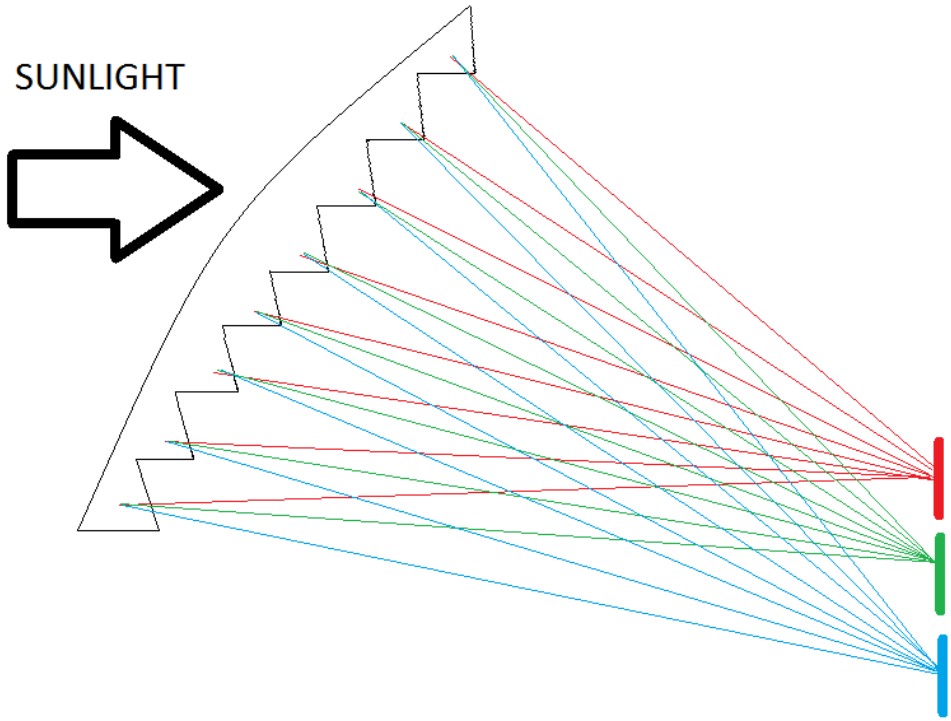

Figure 6: Refractive Spectrum Splitting

2.1.3 Selective Transmission/Reflective Splitting

Some optical filters allow the selective reflection or transmission of different wavelengths of light (e.g. interference based dichroic filters, absorption filters, rugate filters, guided mode resonance filters etc). This selectivity has been used in various geometries with multijunction photovoltaics for concentration as well spectrum splitting, mostly with the types of filters that do not result in significant loss of energy.

One commonly studied design uses a reflective interference (dichroic) filter which splits the incoming light split into two beams. The beam with the band of shorter wavelength is reflected to a wider band gap top cell and the longer wavelengths were transmitted to a shorter band gap cells.

One series of studies [13], [14] explores this design with two combinations of cells. The dichroic filter consisted of multi-layered dielectric oxides with high (n~1.9–2.2) and low (n~1.5) refractive indices. It was fabricated using sputter deposition. The cut-off wavelength was controlled by varying the number of stacking layers as well as their thicknesses. Devices with cut-off wavelengths of 550 nm, 600 nm and 640 nm were designed. The software, “The Essential Macleod” (developed by Thin Film Center, Inc.) was used for the design and optimization of the multi-layered filter.

With a 550nm cut-off and an a-Si top cell, the efficiency was reported to be 25%, while a perovskite top cell yielded a total device efficiency of 28%. (A monocrystalline Si HJ cell was the bottom cell in both cases). The individual cells lost significant current density and efficiency with the spectrum splitting devices, though the overall device efficiencies were still higher than any individual cell's efficiency. The authors asserted that the total efficiency of the optical splitting system could be further improved by increasing the open circuit voltage (V_{oc}) of the top cell with appropriate light management and the efficiency would increase to above 30%.

Green et. al. devised and tested a system with selective reflection, which was combination of stacked multijunction (GaInP and GaInAs grown on Germanium) with a separate silicon cell [15], [16]. The Silicon cell had dichroic band pass filter over it, which only allowed wavelengths between ~850 nm and 1100 nm to travel onwards to the Si cell. The remaining wavelengths were reflected towards the Ge/GaInP/GaInAs multijunction. The authors' purpose was to utilize the part of the spectrum not being utilized efficiently by the stacked triple junction alone. This is evident from the fact that the spectral responsivity of Germanium as a standalone cell is much higher and the excess current is wasted in the stacked multijunction. However, the introduction of Silicon as a separate cell utilizes a part of the wasted power and the relative output power increased by 9%, from 36.8% to 40.1%. The filter consisted of 158 alternating layers of Nb_2O_5 and SiO_2 with a total thickness of 20 um [16].

Another recent example that utilized reflection in a slightly different manner was explored by Ayala et. al. [17] which had a parabolic arrangement of the primary low band gap (Si) PV cells. The surfaces of these cells were covered with holographic optical elements (HOEs) made in dichromated gelatin (DCG), which transmitted longer wavelengths at the Si PV cells while reflecting the shorter wavelengths to a secondary, higher bandgap cell (GaAs). (planar holographic elements that only reflect and focusing is due to the shape while reflective holographic focusing filters to reduce area and increase concentration on higher bandgap cell(s) even further). Due to the parabolic shape, the reflected wavelengths were concentrated at the higher band gap cell(s). The back contacts of the Si cells were modified to improve light trapping. (Possible use of thin film Si cells). By modifying the concentration ratio and filtering properties of the HOE, the system can be optimized for different diffused and direct irradiance based on geographical locations. FRED was used the performance

evaluation of the segmented parabolic concentrator using non-sequential ray tracing, while RCWA using RSoft is used for the simulation of the holographic grating.

The design is tested in three cities in different states in the US, with varying number of segments (6, 10 and 14) in the parabolic reflector arrangement. The simulations show that generally the normalized spectral irradiance on the secondary cell increases as the number of Si PV segments in the parabola are increased. While the HOE systems increase the secondary cell's (GaAs) insolation conversion significantly, they reduce the Si cell's insolation conversion efficiency compared to non-HOE systems, though the overall efficiency increases for both 6 and 10 segment systems. However, overall, the greatest gains in all three cases are seen when six segment parabolic reflectors are combined with Spectrum Splitting HOE.

Overall, the highest conversion efficiency was obtained for 14 segment systems with HOE (27%), though the gain was quite small for the same system compared to its non-HOE counterpart.

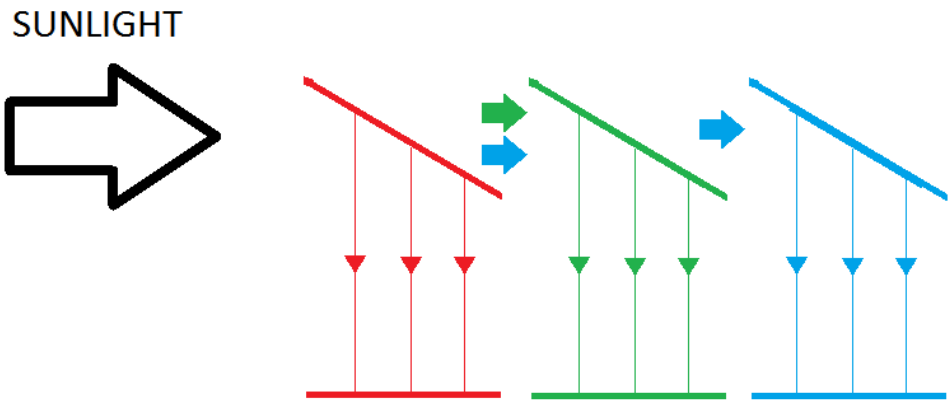

Figure 7: Reflection based spectrum splitting

2.1.4 Diffractive Splitting

Diffraction is the tendency of waves to spread out around obstacles, apertures or as they travel farther from a finite source. The extent to which this happens is dependent on the wavelength, so diffraction is used for dividing a given spectrum in a number of applications. Usually, a periodic arrangement of obstacles/apertures or periodic contrast in the refractive index across a surface is made, which results in the required separation. Such periodic structures are called diffraction gratings. There a number of different arrangements in which they are used in the context of spectrum splitting for photovoltaics. These include the combination of a diffraction grating and a Fresnel

lens (for focusing) on the two separate surfaces of an optical element (called double sided grating Fresnel, or G-Fresnel),[18] superposition of surface profile of a grating over that of a Fresnel lens (single sided G-Fresnel),[19] different configurations of holographic elements[20] or in combination with other optical phenomena [21].

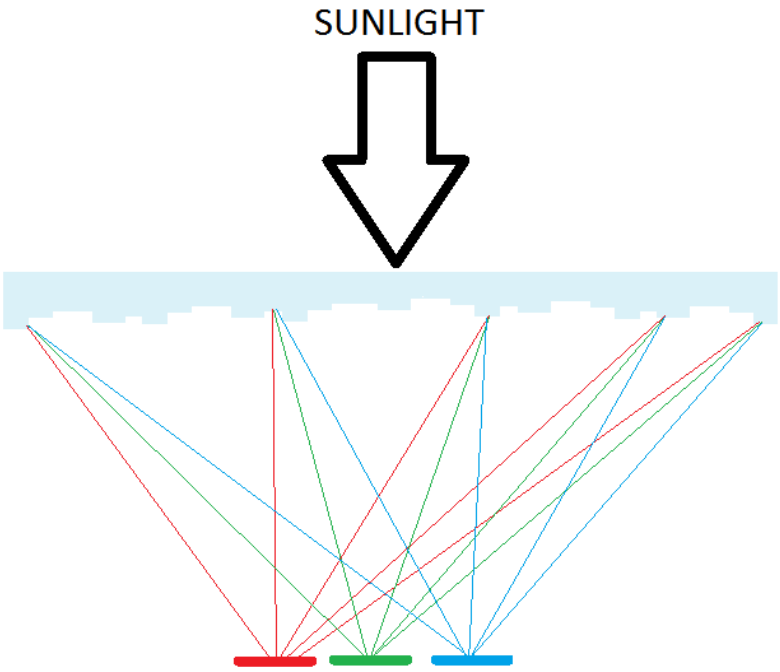

Figure 8: Diffraction based spectrum splitting

This study focuses on the design of a diffraction-based system due to a number of inherent advantages. Diffractive optical elements (DOEs) are compact, both in their form and the dimensions required for their operation, when compared to the other splitting methods. This makes them compatible with the commonly used planar cell geometries [22] that makes them easier to use and install on larger scales. Diffractive elements can also combine splitting and focusing into the same element (called Spectrum Splitting Beam Concentration, SSBC) efficiently, while maintaining their largely planar arrangements. Due to the focus of this work on diffraction, the following section explores the diffraction-based designs reported in recent literature. Studies related to spectrum splitting methods (for solar power in general) from the period preceding 2004 are covered in a comprehensive review by Imenes and Mills [6]. The literature from then till 2012 is reviewed well by Mojiri et al [23].

2.2 Overview of Recent Literature Utilizing Diffraction for Spectrum Splitting

2.2.1 Double and Single Sided Grating Fresnel

In a double-sided G-Fresnel, the splitting and focusing power of the optical element exists on its two separate surfaces. While two different surfaces have to be catered for, each individual surface is simpler to design and manufacture (fewer chances of imperfections) when compared to a single sided G-Fresnel. Michel et al [24] designed such a double sided G-Fresnel for SSBC, focused on space-based PV . The visible wavelengths are diffracted into the 1st order, where a GaAs cell was placed and the IR wavelengths were focused on a Germanium cell placed at the 0th order. The optimized design with a symmetric profile utilized a blazed grating, with a blaze wavelength of 560nm and a period of 22um. The focal length for separation was 75mm with an f-number of 3. The optical element was designed with Silicone DC93-500 as the material, which is one of the standards for space applications.

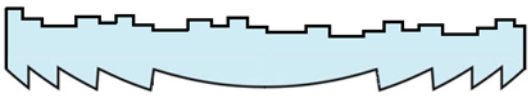

Figure 9: A general example of a double-sided grating-Fresnel

The design was simulated using the scalar diffraction theory and ray-tracing, considering AM0 irradiance. The design was found to achieve an optical efficiency of 76.5%, resulting in a power output of 288 W/m^2. The concentration ratio of the radiation over the 4.9mm wide Ge cell was 10.2x and 13.7x on the 7.3mm wide GaAs cell. Due to the concentration, the cells could reach temperatures of up to 70 ^{o}C. In subsequent papers [25] [26], Michel et al. investigated two modifications to this design. The blazed grating was further optimized by introducing a variable grating period (20um to 30um) and a different design wavelength (450nm) to achieve better concentration. The second modified design used a lamellar grating instead of a blazed one (also with varying grating period), which focused most of the power in the ±1 orders, but with much sharper cut-offs, thereby achieving better performance. As a result, the combination of cells had to be different for the design with lamellar grating. The lamellar grating's period varied between 34um and 23um, with a design wavelength of 480nm. For these designs, the simulations were first run using scalar

diffraction theory and ray-tracing, though the final grating designs were simulated more rigorously using PC-Grate. The simulations for temperature measurements were made using ESATAN. Both the optimized designs had the following the parameters.

	Blazed	**Lamellar**	**GaAs (or non-splitting element)**
Optimal bandgaps	0.95, 1.65 eV	1.15, 1.9 eV	1.42
Design Wavelength	450nm	480nm	-
Grating variation	Between 20um & 30 um	34um to 23um	-
C_{geo} (post-optimization)	12 and 16	8.3 and 16.3	11x
90% power tolerance angle	0.8^o	0.7^o	0.85^o
Temperatures	68^o and 72^o	67^o and 63^o	80^o and 84^o

Table 1: Comparison of Blazed and Lamellar grating-based designs by Michel et al

In comparison with a single junction cell and comparable stacked multijunctions, these designs performed as follows.

	SJ (GaAs)	**DJ (InGaP/GaAs)**	**TJ (InGaP/GaAs /Ge)**	**Blazed (3MJs)**	**Lamellar (3MJs)**
P_{out} (W/m^2)	282	317	354	287	299

Table 2: Power output of various multijunctions compared to Michel et al splitting system

While the lamellar configuration performed better than a SJ under concentration, the blazed grating design had a lower power output. While the proposed designs could not beat the performance of the conventional DJ and TJ designs, they did have some

potential advantages over the proposed designs. These advantages included cheaper cells, more possible combinations of cells, use of AR coatings for relevant spectrums ensuring lower reflections and higher tolerance to degradation due to lower operational temperatures under the same conditions.

Albarazanchi et al. [19] studied the design of a single sided G-Fresnel which was modeled at the subwavelength level. The ability to diffract and focus from a single surface was achieved by the superposition of a grating over the surface profile of a Fresnel lens. The surface profile was then quantized and converted to a binary grating using effective medium theory.

Two devices were designed with subwavelength grating periods of 0.25um and 0.45um, with diameters of 1cm and 1.5 cm for the Fresnel lens. Focal lengths for both were 50cm and the design wavelength was 9um. The refractive index was chosen to be 1.46 for both devices. The target was to split incoming solar radiation into two bands, 0.4 to 1.1 um and 1.1 to 1.5um, where two solar cells could be placed. The cell widths would need to be 0.3655 cm and 0.3646 cm for the first model and 0.5444cm and 0.5518cm for the second model. Separation from solar cells would be 40.8 cm and 40.9 cm respectively for each model.

For design and simulation, FDTD was used for the near field within the thickness of the device using MEEP (it was also used during the design phase) while Angular Spectrum Method (ASM) was used for propagation from the output plane of the element to the plane of the cells. This combination of the two numerical methods was used to save computation time.

The authors used a metric called "Optical concentration factor" (C_{opt}) to measure the devices' performance (the product of geometric concentration ratio and optical efficiency, both taken as functions of wavelengths). C_{opt} was calculated by averaging its value over different wavelengths (0.4 to 1.5um in steps of 0.1um). C_{opt} was between 70-6.6e^3 and 121-7.052e^3 for the two PV cells for the first device model while 99.63 - 9132e^4 and 67.88 - 10.335e^4 for the second model.

A subsequent modification [27] on the design changed the operational wavelength to the more practical range of 400nm-1100nm, by splitting it into two bands (400-800 and 800-1100).

The multilevel grating profile was similarly converted into an equivalent binary grating with 4 and 8 levels. This was again based on an FDTD based numerical analysis and a combination of FDTD and ASM was then used to the analyze the performance of the model.

The optical concentration factor for this design was ~70% for both bands for the 8-level device and ~70% and ~56% for the 4-level device for the shorter and longer bands respectively.

This lens to split the 400-1100nm band into 400-800nm and 800-1100nm bands was then fabricated and experimentally verified [28].The design wavelength was 0.6 μm, with a focal length of ~15 cm and a lens diameter of 1 cm. It was fabricated with direct laser writing grayscale lithography and the surface was characterized with a Zygo profilometer. The measured optical efficiencies were then ~58% in both bands rather than the simulated 70% and 52% expected from the simulation results. The authors attributed the large disparity between simulated and measured performances to the effect of quantization of the surface profile and the fabrication tolerances.

Another class of single sided G-Fresnel designs use a different design methodology for combining diffractive and focusing power in a single surface profile. The design phase usually starts with a separate focusing lens and grating to achieve the desired splitting. The lens is then converted to an equivalent Fresnel lens by using the fact that effect of the surface profile repeats with each phase differences of 2π. The same rule is used to find a surface thickness function that corresponds to the combined surface profile of the G-Fresnel formulated in the previous step. This step often uses search algorithms to come up with a unique surface profile to achieve the required focusing and separation. By varying the bandwidths, error/merit functions and search algorithms for the optimization of the surface profile, a number of different devices have been designed and simulated.

Jin-Ze et al [29] detailed three surface thickness optimization algorithms which generated surface profiles for an SSBC diffractive optical element. Each algorithm was characterized by a different error function. These algorithms introduced two different error functions which considered the different effect of thickness on the complex amplitudes of different wavelengths of incoming light and the contributions of different wavelengths to the overall efficiency by giving them weightage. Each error

function considered different parameters for optimization, so there was difference in their efficiencies across different wavelengths. Though the study focused on the error function which considered the different effect of thickness on the complex amplitudes of different wavelengths. Three factors of design wavelengths choice were studied against their effect on overall efficiency, (i) number of design wavelengths (ii) their coverage range and (iii) intervals between them. The authors found that higher numbers of design wavelengths didn't necessarily increase the optical efficiency. 3 to 8 design wavelengths were used and 5 gave the highest efficiency. Larger coverage range with uniform intervals between design wavelengths also didn't necessarily yield higher efficiencies.

Increasing the maximum phase also showcased increase in optical efficiency at least between 18π and 100π, where 100π approaches the optical efficiency of the ideal form (ideal, as in the original equation before "optimization" algorithm starts working on it). The resulting design's average optical efficiency was approximately 6.8% higher than that of the previous design [30].

Dong-Feng et al [31] continued with the same design methodology, quantizing the surface profile to 32 levels. The design aimed at dividing the incoming spectrum into three bands 400-500nm, 500-600nm and 600-700nm, with corresponding design wavelengths of 450nm, 550nm and 650nm. The design was fabrication is carried out using a "five-cycle reactive ion etching". In each cycle the quartz substrate was (i) cleaned rigorously, (ii) spin coated with photoresist, (iii) photoresist was exposed to UV light with mask to fabricate patterns, (iv) O_2 plasma reactive etched to remove residual photoresist, (v) required pattern etched on quartz using the pattern in the photoresist (vi) removal of photoresist. The design wavelengths were generated using a Nd:YAG laser and further optics to create a specific window of light. (21.22mm here)

The system reached a concentration factor of 12X and average optical efficiency is 60.07% for the three design wavelengths. The width of each sub-spectrum for each target solar cell was 1.76mm.

Li et al [32] investigated the use of simulated annealing as the optimization algorithm for generating the required surface profile. Using the same focal length and design

wavelengths, the sizes of input and output planes were 21.23mm and 5.31mm and quantized to 4096 pixels, with fused silica (n = 1.46) as the material.

The parameters varied during the design optimization process included the maximum permitted phase (between 2π and 32π), the quantization level number (between 16 and 64), the input pixel number (between 512 and 8192) and the target focusing region width (1.04mm to 0.065mm). The focusing efficiency, was at a maximum of approximately 60% but the author's suggested values to balance fabrication ease with performance gave 56%. The numerical results were calculated using the Fresnel diffraction integral, which revealed that generally, increase in the quantization levels and maximum permitted phase generally improved the focusing efficiency.

Xu et al [33] studied a slightly modified version of this method in which they started by combining a different grating with the focusing lens for each design wavelength, rather than the one combination for all. This was expected to increase focusing efficiency as the grating component would be according to design wavelengths and allow arbitrarily presetting focal positions. The resulting optical focusing efficiencies were 60.18%, 62.85% and 78.25% for design wavelengths of 0.45, 0.55 and 0.65 um with an average of 67.09%.

2.2.2 Holographic Optical Elements

Holographic Optical Elements (HOEs) are optical elements that are produced using holographic imaging processes. The advantages often cited in using holographic systems include up to 100% diffraction efficiency in a single order, complex functions can readily be recorded, are dispersive, have low scatter, can record high spatial frequencies with corresponding large diffraction angles and they have been shown to be mass producible in large quantities at low cost. As a result, they have been studied extensively for combining spectrum separation and concentration in a single element.

Vorndran et al [34] [35] presented a transmissive, volume holographic lens (VHL) for spectrum splitting into two bands targeting Si and InGaP cells. Utilizing the angular Bragg selectivity of a holographic grating, direct normal irradiance (DNI) was diffracted into a specified angle while the diffused irradiance was incident at angles that passed through the hologram. The diffracted light was focused by varying the grating period across the aperture of the VHL. The primary performance metric used here was the Improvement over Best Band Gap (IoBB), which is the ratio of increased

PCE of the multijunction device to the PCE of the single junction with the best power output, considering both of them covering the same area.

The VHL design was optimized for high diffraction efficiency using Kogelnik's Coupled wave theory for thick holograms [36]. The resulting system had a height of 1cm, unit width of 1.29cm and the holographic film had a thickness of 20um. The holographic lens was recorded in dichromated gelatin (DCG) and its average first-order diffraction efficiency was 85.4% at 532 nm. This resulted in a PCE of 30.2%, despite the very low geometric concentration ratios of 2.43x and 1.70x over InGaP and Si respectively. This meant it had achieved an IoBB of 15% (compared to the simulation's expectation of 19.7). An ideal filter with the same parameters would have had an IoBB of 24%.

The authors suggested that improvements were possible by segmenting the aperture and controlling the exposure parameters during holography, to optimize the index modulation across the aperture. They also suggested tuning the peak diffraction wavelength, improving the peak diffraction efficiency (DE) values and reducing the absorption and scattering of light in the film. Peak DE values can be improved by optimizing exposure energy across the holographic lens. Scattering can be reduced by making changes to the fabrication process of the holographic film. The authors also noted that improvement over best band gap was affected by the variation in irradiance patterns at different locations within the United States of America.

Ingersoll et al [37] investigated the combined use of two holographic gratings and compared two different configurations for it. As a single element (both grating profiles multiplexed) and a "sandwiched-grating" arrangement, where one followed the other independently. "Particle swarm optimization" method was used to optimize both the configurations for spectral separation and optical designs showed performance enhancements when compared to single-grating solutions. The sandwiched-, multiplexed-, and single-grating systems exhibited efficiencies of 82.1%, 80.9%, and 77.5%, respectively, (in comparison with an ideal bandpass spectrum splitter). The authors suggested that the dispersion performance could be improved even further if more than two gratings were utilized in the spectrum splitter, but the additional cross-coupling would decrease the efficiency. It was observed that the multiplexed-grating systems were more susceptible to this.

Chrysler et al. [38] devised a spectrum-splitting system based on volume holographic lenses (VHL) with a noteworthy layout. A GaAs cell was positioned at the centre of the device, two Si cells on either side. The holographic device above them was a side by side combination of four holographic lens segments. Each had a different profile, diffracting the required wavelengths to the respective cells. Segments that were positioned over silicon and were designed to diffract most efficiently in the GaAs spectral band (350-875nm), whereas segments positioned over GaAs were designed to diffract most efficiently in the Silicon spectral band (875-1200nm). This arrangement ensured that all the area under the optical element could be populated with cells, despite the off-axis nature of diffraction. Furthermore, only each segment's high diffraction efficiency band needs to be used.

The improvement in total power output was expected to be 15.2% compared to a non-spectrum-splitting reference using simulations with a ray tracing model in FRED. The lens was fabricated in Covestro Bayfol HX photopolymer by combining lens segments through sequential masked exposures. The measurement-based improvement in power output was determined to be 8.5%.

Wu and Kostuk [39] described another holographic splitting system for a two-junction PV device that uses GaAs and Si PV cells arranged in alternating patches of unequal widths. The splitting system combined a high efficiency grating with an array of micro-lenses for the focusing function. Longer wavelengths (880nm to 1200nm) were diffracted into the first order to narrow bandgap cells (Si) while the shorter wavelengths (300nm to 880nm) focused onto the wide bandgap cells (GaAs) lying in the zeroth diffraction order. The performance of the system was simulated with a non-sequential raytracing model, (considering the properties of DCG) using Photon Engineering FRED Optimum, while the diffraction efficiencies for different wavelengths and incident angles of the holographic filters were calculated with RCWA using RSoft DiffractMOD.

Micro-lenses with F# = 1 and 1.5 were explored and F#=1.5 had better results. The average diffraction efficiency was 90% in the bandwidth of interest (900nm to 1200nm). The results showed that the proposed system could reach conversion efficiencies of 31.98%, which corresponded to an IoBB of 20.05% and had an acceptance angle of ± 6 degrees.

A 2018 paper by Wu et al [20] detailed the design, optimization and fabrication of another transmissive holographic element in DCG for two and three junction PV cells, in both single element and cascaded filter configurations. Though the focus of analysis was on the three-junction device. The design was optimized using a search algorithm to tune the parameters of the holographic element to maximize the "system optical factor" (SOF), which considers the optical fill factor (OFF) and the band gap of cells.

The simulated two-junction devices had system power efficiencies of 40.97% and 42.56% for single and cascaded filters respectively, while the three-junction systems had power efficiencies of 45.77% and 48.41% for single and cascaded filters respectively. In both cases the cascaded filters even beat the reference multijunction cells taken for comparison. The cascaded three junction model was consequently recorded in DCG. The measurements of transmittance spectra through this device was used to calculate diffraction efficiencies, from which the PCE was calculated to be 46.93% (compared to the simulated value of 48.41%).

It is evident from this discussion that holographic optical elements have shown great promise in their performance as spectrum splitters for PV, in addition to their aforementioned qualities. However, holographic media degrade rapidly, especially in the harsh conditions under solar insolation. As such their stability needs to improve if they are to be practically useful. The degradation of two common holography materials in possible operational conditions was investigated by Chrysler et al [40]. Diffraction gratings recorded in Covestro Bayfol HX photopolymer and DCG (along with a polymer based, reflective 3M dichroic filter for comparison) were encased in glass plates and placed in the open in Tucson, Arizona, USA for a total of 16 weeks. Even for the limited time duration of 16 weeks, the Bayfol HX polymer showed more than 22% degradation in diffraction efficiency, up to 43% increase in absorption of certain wavelengths (400nm), change in spectral bandwidth and Bragg angle and an increase in film thickness. DCG had lesser losses in diffraction efficiency (2-3%), change in spectral bandwidth, but significant reduction in film thickness (4.5%). The stability of holographic materials for use in solar panels is therefore an active area of research.

2.2.3 Combination of diffractive elements with waveguides

Blain et al [41] studied the combination of a Grating-Fresnel with a waveguide. Unlike a normal G-Fresnel, the separated beams were incident on a waveguide. The back side

of the waveguide had V-shaped grooves that were coated with aluminium. By virtue of the positioning of the grooves, the incoming split beams were reflected in different directions and propagated through the waveguide via TIR onto their respective PV receivers.

The blazed grating, waveguide, grooves and their positions were chosen with the aim of having spectrum splitting that matched the respective dye sensitized cells (a 400nm-600nm band and a 600-700nm for the relevant cells). The blazed grating master had a fixed period of 22.22 μm with a blaze angle of 2.22°for the blaze of wavelength 500 nm. The authors suggested that the master could be reproduced in PMMA through nanoimprint lithography, which would be more suitable for mass production.

The focusing surface was a cylindrical Fresnel lens, which compelled the light to propagate in only two directions inside the waveguide and each one lead to a different DSSC. The lenses were designed to be asymmetric so that they let the unwanted 0th order pass through the waveguide to avoid overheating the system. The final lens design had a back focal length of 20 mm and a focal point offset of 1.1 mm. Five (5) of these lenses (10×20 mm^2) were used and thus the dimensions of the overall slab were 50×20×5 mm. The positions of the aluminium coated V-grooves inside the waveguide were chosen to focus the central wavelength (600 nm) at the top of each groove.

In a subsequent publication [21], this planar splitter/concentrator was realized in PMMA and the performance was investigated using simulations and the fabricated system.

Theoretical optical efficiency of 73% was achieved while the experimental result was 55%, despite good individual lens and grating performing. Most of the optical losses were experienced after the grating/lens pair was combined with the waveguide. The losses were identified by the authors experimentally, with most of them due to diffraction (45%), reflection (15%+4%) and decoupling from waveguide (17.5% in spite of the identified factors and compromises made in design). Also, the DSSCs were unstable during the experiment, so the PCE was even lower. The study was rigorous and important to understand the different effects surrounding this design type to further improve this technique.

As discussed, the instability of holography materials (such as dichromated gelatin, DCG) is a serious challenge [40] and an active area of research. Single-sided G-Fresnel might be easier to integrate over lateral MJ cells (as one side can be flat), but their surface profiles are complicated to design as well as manufacture. This can result in higher costs and lower efficiency due to imperfections in the final product. While the surface profiles of both sides of a double-sided G-Fresnel have to be given attention for the operation of the system, they are still compact and easier to design. Therefore, this study discusses a design methodology consisting of a two-element spectrum splitting system that is easier to design and implement using more commonly available components for quick prototyping and testing in a lab. This system could then be extended to achieve a double-sided G-Fresnel.

2.3 SUMMARY

This chapter on literature review looked into the different types of designs in literature for solar spectrum splitting targeted at photovoltaics. The designs were categorized according to the optical techniques used for spectrum splitting, i.e. luminescence, selective reflection, refraction and diffraction. The pros and cons of each category of techniques were studied and it was decided that diffraction was to be pursued to achieve the objectives of this thesis. Diffractive spectrum splitting designs were then investigated in further detail and divided into categories for ease of examination. Having considered all these reported designs, the target for design was set to be a two-component diffraction based splitting system.

2.4 REFERENCES

[1] E. D. Jackson, “Areas for improvement of the semiconductor solar energy converter,” presented at the *Conference on Solar Energy: The Scientific Basis*, Tucson, AZ, USA, 1955.

[2] W. H. Weber and J. Lambe, “Luminescent greenhouse collector for solar radiation,” *Appl. Opt.*, vol. 15, no. 10, pp. 2299–2300, 1976.

[3] A. Goetzberger and W. Greube, “Solar energy conversion with fluorescent collectors,” *Appl. Phys.*, vol. 14, no. 2, pp. 123–139, Oct. 1977.

[4] A. Zastrow, “The Physics and Applications of Fluorescent Concentrators - A Review,” in *Proceedings of SPIE Volume 2255, Optical Materials Technology for Energy Efficiency and Solar Energy Conversion XIII*, 1994, Freiburg, Germany, vol. 2255.

[5] B. Fisher and J. Biddle, “Luminescent spectral splitting: Efficient spatial division of solar spectrum at low concentration,” *Solar Energy Materials and Solar Cells*, vol. 95, no. 7, pp. 1741–1755, Jul. 2011.

[6] A. G. Imenes and D. R. Mills, “Spectral beam splitting technology for increased conversion efficiency in solar concentrating systems: a review,” *Solar Energy Materials and Solar Cells*, vol. 84, no. 1–4, pp. 19–69, Oct. 2004.

[7] Francesco Meinardi, Samantha Ehrenberg, Lorena Dhamo, Francesco Carulli, Michele Mauri, Francesco Bruni, Roberto Simonutti, Uwe Kortshagen & Sergio Brovelli “Highly efficient luminescent solar concentrators based on earth-abundant indirect-bandgap silicon quantum dots,” *Nature Phototnics*, vol. 11, no. 3, pp. 177-185, 2017.

[8] Kaifeng Wu, Hongbo Li & Victor I. Klimov, “Tandem luminescent solar concentrators based on engineered quantum dots,” *Nature Photonics*, vol 12, no. 2, pp. 105-110, January 2018.

[9] R. W. Olson, R. F. Loring, and M. D. Fayer, “Luminescent solar concentrators and the reabsorption problem,” *Appl. Opt.*, vol. 20, no. 17, pp. 2934-40, Sep. 1981.

[10] M. Stefancich, A. Zayan, M. Chiesa, S. Rampino, L. Kimerling, and J. Michel, “Single element spectral splitting solar concentrator for multiple cells CPV system,” *Optics Express*, vol. 20, no. 8, pp. 9004-9018, 2012.

[11] C. Maragliano, M. Chiesa, and M. Stefancich, “Point-focus spectral splitting solar concentrator for multiple cells concentrating photovoltaic system,” *Journal of Optics*, vol. 17, no. 10, p. 105901, 2015.

[12] C. Maragliano, H. Apostoleris, M. Bronzoni, S. Rampino, and M. Chiesa, “Efficiency enhancement in two-cell CIGS photovoltaic system with low-cost optical spectral splitter,” *Optics Express*, vol. 24, no. 2, pp. A222-A233, 2016.

[13] K. Yamamoto Daisuke Adachi, Hisashi Uzu, Mitsuru Ichikawa, Toru Terashita, Tomomi Meguro, Naoaki Nakanishi, Masashi Yoshimi and José Luis Hernández, “High-efficiency heterojunction crystalline Si solar cell and optical splitting structure fabricated by applying thin-film Si technology,” *Jpn. J. Appl. Phys.*, vol. 54, no. 8S1, p. 08KD15, Aug. 2015.

[14] H. Uzu, Mitsuru Ichikawa, Masashi Hino, Kunihiro Nakano, Tomomi Meguro, José Luis Hernández, Hui-Seon Kim, Nam-Gyu Park and Kenji Yamamoto, “High efficiency solar cells combining a perovskite and a silicon heterojunction solar cells via an optical splitting system,” *Applied Physics Letters*, vol. 106, no. 1, p. 013506, 2015.

[15] M. A. Green, M.J. Keevers, B. Concha-Ramon, Y. Jiang, I. Thomas, J.B. Lasich, P.J. Verlinden, Y. Yang, X. Zhang, K. Emery, T. Moriarty, R.R. King, W. Bensch, “Improvements in Sunlight to Electricity Conversion Efficiency: Above 40% for Direct Sunlight and over 30% for Global,” *Proceedings of 31st European Photovoltaic Solar Energy Conference,* Hamburg, Germany, 14-18 Sep. 2015.

[16] M. A. Green, M. J. Keevers, I. Thomas, J. B. Lasich, K. Emery, and R. R. King, “40% efficient sunlight to electricity conversion: Sunlight to electricity conversion efficiency above 40%,” *Progress in Photovoltaics*, vol. 23, no. 6, pp. 685–691, Jun. 2015.

[17] S. A. Pelaez, S. Vorndran, Y. Wu, B. Chrysler, and R. Kostuk, “Segmented holographic spectrum splitting concentrator,” in *Proceedings of SPIE 9937 Next*

Generation Technologies for Solar Energy Conversion VII, San Diego, USA, vol. 9937, 23 Sep. 2016.

[18] C. Michel, "Optical study of a solar concentrator for space applications based on a diffractive/refractive optical combination," *Solar Energy Materials and Solar Cells, vol. 120, pp. 183-190,* 2013.

[19] A. Albarazanchi, P. Gerard, P. Ambs, and P. Meyrueis, "Design of single layer subwavelength diffractive optical element (G-Fresnel) for spectrum splitting and beam concentration," *Proc. SPIE 9131, Optical Modelling and Design III, 913126*, Brussels, Belgium, 2014.

[20] Y. Wu, B. Chrysler, and R. K. Kostuk, "Design and fabrication of cascaded dichromate gelatin holographic filters for spectrum-splitting PV systems," *Journal of Photonics for Energy*, vol. 8, no. 1, p. 017001, 2018.

[21] C. Michel, Pascal Blain, Lionel Clermont, Fabian Languy, Cédric Lenaerts, Karl Fleury-Frenette, Marc Décultot, Serge Habraken, Denis Vandormael, Rudi Cloots, Gopala Krishna V.V. Thalluri, Catherine Henrist, Pierre Colson, JérômeLoicq, "Waveguide solar concentrator design with spectrally separated light," *Solar Energy*, vol. 157, pp. 1005-1016, 2017.

[22] C. Michel, J. Loicq, T. Thibert, and S. Habraken, "Optical study of a spectrum splitting solar concentrator based on a combination of a diffraction grating and a Fresnel lens," *AIP Conference Proceedings*, vol. 1679, no. 1, 070002, 2015.

[23] A. Mojiri, R. Taylor, E. Thomsen, and G. Rosengarten, "Spectral beam splitting for efficient conversion of solar energy—A review," *Renewable and Sustainable Energy Reviews*, vol. 28, pp. 654–663, Dec. 2013.

[24] C. Michel, J. Loicq, F. Languy, and S. Habraken, "Optical study of a solar concentrator for space applications based on a diffractive/refractive optical combination," *Solar Energy Materials and Solar Cells*, vol. 120, pp. 183–190, Jan. 2014.

[25] C. Michel, J. Loicq, T. Thibert, and S. Habraken, "Optical study of diffraction grating/Fresnel lens combinations applied to a spectral-splitting solar concentrator for space applications," *Appl. Opt.*, vol. 54, no. 22, p. 6666, Aug. 2015.

[26] C. Michel, J. Loicq, T. Thibert, and S. Habraken, “Optical study of a spectrum splitting solar concentrator based on a combination of a diffraction grating and a Fresnel lens,” in *AIP Conf. Proc. 1679*, Aix-les-Bains, France, 2015, pp. 070002-1-070002–7.

[27] A. Albarazanchi, P. Gérard, P. Ambs, and P. Meyrueis, “Alternative model of a Subwavelength Diffractive Lens (SWDL) proposed for PV cells applications,” *IEEE Photonics Technology Letters*, vol. 27, no. 12, pp. 1317-1320, 2015.

[28] A. Abbas, P. Gerard, P. Ambs, P. Meyrueis, G. N. Nguyen, and K. Heggarty, “A smart multifunction diffractive lens experimental validation for future PV cell applications,” *Optics Express,* vol. 24, no. 2, pp. A139-145, 2016.

[29] W. Jin-Ze *et al.*, “Design optimization of highly efficient spectrum-splitting and beam-concentrating diffractive optical element for lateral multijunction solar cells,” *Chinese Physics B,* vol. 23, no. 4, p. 044211, 2014.

[30] Y. Jia-Sheng, W. Jin-Ze, H. Qing-Li, D. Bi-Zhen, Z. Yan, and Y. Guo-Zhen, “A single diffractive optical element implementing spectrum-splitting and beam-concentration functions simultaneously with high diffraction efficiency,” *Chinese Physics B,* vol. 22, no. 3, p. 034201, 2013.

[31] Dong-Feng Lin, Bao-Gang Quan, Qiu-Lin Zhang, Dong-Xiang Zhang, Xin Xu, Jia-Sheng Ye, Yan Zhang, Dong-Mei Li, Qing-Bo Meng, Li Pan and Guo-Zhen Yang “Spectrum-Splitting Diffractive Optical Element of High Concentration Factor and High Optical Efficiency for three junction PV,” *Chinese Physics Letters* vol. 33, no. 9, p. 094207, 2016.

[32] J. Li, Wen-Qi Xu, Jia-ShengYe, Peng Han, Wen-Feng Sun, Sheng-Fei Feng, Xin-Ke Wang, Yan Zhang, “High focusing efficiency or high signal-to-noise ratio diffractive optical element for color separation and light focusing,” *Optik,* vol. 138, pp. 87-94, June 2017.

[33] W.-Q. Xu, Dong-Feng Lin, Xin Xu , Jia-Sheng Ye, Xin-Ke Wang, Sheng-Fei Feng, Wen-Feng Sun, Peng Han, Yan Zhang, Qing-Bo Meng and Guo-Zhen Yang “Simple and universal method in designs of high-efficiency diffractive optical elements for spectrum separation and beam concentration,” *Chinese Physics B,* vol. 26, no. 7, p. 074202, 2017.

[34] S. D. Vorndran, L. Johnson, T. Milster, and R. K. Kostuk, “Measurement and Analysis of Algorithmically-Designed Diffractive Optic for Photovoltaic Spectrum Splitting,” Proceedings of *2016 IEEE 43rd Photovoltaic Specialists Conference (PVSC),* 5-10 June 2016, Portland USA.

[35] S. D. Vorndran, B. Chrysler, B. Wheelwright, Z. Holman, and R. Kostuk, “Off-axis holographic lens spectrum splitting photovoltaic system for direct and diffuse solar energy conversion,” *Applied Optics*, vol. 55, no. 27, pp. 7522-7529, 2016.

[36] H. Kogelnik, “Coupled Wave Theory for Thick Hologram Gratings,” *The Bell System Technical Journal*, vol. 48, no. 9, pp. 2909–2947, Nov. 1969.

[37] G. B. Ingersoll and J. R. Leger, “Optimization of multi-grating volume holographic spectrum splitters for photovoltaic applications,” *Appl. Opt.*, vol. 55, no. 20, p. 5399, Jul. 2016.

[38] B. D. Chrysler, Y. Wu, Z. Yu, and R. K. Kostuk, “Volume holographic lens spectrum-splitting photovoltaic system for high energy yield with direct and diffuse solar illumination,” *Proc. SPIE 10368, Next Generation Technologies for Solar Energy Conversion VIII,* 103680G (25 August 2017).

[39] Y. Wu and R. K. Kostuk, “Two-junction holographic spectrum- splitting microconcentrating photovoltaic system,” *Journal of Photonics for Energy*, vol. 7, no. 1, p. 017001, 2017.

[40] B. D. Chrysler, S. Ayala Pelaez, Y. Wu, S. D. Vorndran, and R. K. Kostuk, “Environmental stability study of holographic solar spectrum splitting materials,” *Proc. SPIE 9937, Next Generation Technologies for Solar Energy Conversion VII*, San Diego, California, United States, 99370N (23 September 2016).

[41] P. Blain, C. Michel; L. Clermont; F. Languy; M. Décultot; Serge Habraken; C. Lenaerts; K. Fleury-Frenette; D. Vandormael; Jérôme J. D. Loicq, “Spectral splitting planar solar concentrator: Experimental testing of a design aiming at dye sensitized solar cells,” in *Proc. of SPIE Vol. 9140, Photonics for Solar Energy Systems V*, vol. 9140, p. 91400S 2014.

CHAPTER 3: DESIGN METHODOLOGY

3.1 THEORETICAL BACKGROUND FOR DESIGN

In order to design a diffraction-based system for spectrum splitting of solar radiation for PV, a few areas of optics are discussed here. First, the equations for the design of spherical lenses are briefly discussed. Then the theories that describe diffraction are overviewed. This is followed by short explorations of two types of diffractive optical elements, namely diffraction gratings and zone plates.

3.1.1 Lens maker's equation

The optical phenomenon leveraged to manipulate light with lenses is refraction. In the design considered here, it is used to focus the wavelengths split by to diffraction (discussed ahead). The refraction of light between two surfaces is explained by Snell's law and equivalently, Fermat's principle. Using these laws and building on the simple cases of the thin lens approximation, the equation for the focusing power of a single curved surface is derived to be as follows [1].

$$\frac{1}{f} = \phi = \frac{1}{R}(n' - n^*) = C(n' - n^*) \tag{3.1}$$

As a lens is a combination of two surfaces, the above equation can be used in conjunction with the equation for combining two thin lenses, which is, [1]

$$\phi = \phi_1 + \phi_2 - \frac{d}{n}\phi_1\phi_2 \tag{3.2}$$

The two preceding equations lead to a third very important one called the "Lens Maker's Equation",[1]

$$\phi = \frac{1}{R_1}(n-1) + \frac{1}{R_2}(1-n) + \frac{d}{n}\frac{1}{R_1R_2}(n-1)^2 \tag{3.3}$$

Which can also be represented as,

$$\phi = C_1(n-1) + C_2(1-n) + \frac{d}{n}C_1C_2(n-1)^2 \tag{3.4}$$

This equation is valid for a lens of thickness *d*, made of material with refractive index *n* surrounded by air or vacuum. In the less common case of the lens being surrounded

by another medium, the unity inside the brackets in the equations 3.3 and 3.4 is replaced by the refractive index of that medium. This very important in the design process of practical lenses as it relates the focal length/power of a lens with its curvature, refractive index and thickness. This provides a starting point for designs and also acts as a tool for conversion between theoretical thin lenses and practical thick lenses.

3.1.2 Diffraction and theories of diffraction

As briefly discussed before, diffraction can be defined as the tendency of waves to spread and deviate from a rectilinear path as they traverse through an aperture [2]. The phenomenon is also observed when waves encounter other arrangements of obstacles, changing refractive indices or when they move farther from a finite source. The mechanism of diffraction is explained by physical (wave) optics. At its most basic, it is physically explained by the Huygens-Fresnel principle, which considers all unobstructed points of a wavefront as sources of spherical secondary wavelets, with the same frequency as that of the primary wave. The amplitude of the optical field at any point beyond that is then simply considered the superposition of all the secondary wavelets.

A number of mathematical models of varying complexity and accuracy exist and are used according to requirements. Generally, models of diffraction devised to calculate field intensities at points beyond the aperture are computation intensive even for simple cases. Therefore, approximations are commonly made to decrease the level of complexity of the calculations for easier computations in reduced times. The approximations and assumptions are often based upon the distance between the region of interest and diffracting plane or the relative dimensions of the diffracting aperture and wavelength of light. The models can be divided into scalar and vector theories of diffraction. Scalar diffraction theories describe the field of radiation as a scalar quantity. Their examples are, Fraunhofer, Fresnel-Kirchhoff and Rayleigh-Sommerfeld [2]. Generally, as the approximations reduce the computational complexity, they also reduce the region in which the results of the models are reasonably accurate. For example, the Fraunhofer model (a simpler form of the Fresnel formulation) is one of the simplest in terms of computation when compared to the other models. However, consequent to its assumptions, it is valid when the distance to the

point of interest is particularly far away ($z >> \frac{kr^2}{2}$, called the Far-field region) [3]. This is the region where the shape of the diffracted field doesn't change as the distance from the aperture z increases. Only the dimensions of the shape of the field change.

However, there are applications where the field in the near-field is of interest. The Fresnel formulation is more complicated mathematically, but it is valid from a much shorter distance. The even more complex Rayleigh-Sommerfeld model is valid at even smaller distances than the Fresnel model. As an example, for plane waves with a wavelength of 10μm passing through a circular aperture of radius 100μm, the Fresnel diffraction theory's results are valid from a distance *z* of 200μm after the aperture, while an approximate Rayleigh-Sommerfeld theory's calculations are valid from a distance *z* of 10 μm.

Vector diffraction theories are usually needed for applications where the polarization needs to be considered and when the structures in and around the propagation path of light are around the same size or smaller than the wavelength. As light is a vector electromagnetic wave, it is logical that a vector diffraction theory would give more accurate results in more cases than a scalar diffraction theory [2]. Hertz vector diffraction theory considers field of electric and magnetic fields in terms of Hertz vectors, Π [4]. The electric and magnetic fields at each point have to be determined from the Hertz vector at a corresponding point by calculating the following double integral.

$$\Pi_x(x, y, z) = \frac{iE_o}{2\pi k} \iint \frac{e^{-ik\rho}}{\rho} dx_o dy_o \tag{3.5}$$

For computational simplicity, two single integral forms are then derived for separately calculating field components within the geometric shadow of the aperture and the geometrically illuminated region.

Whereas the Hertz vector diffraction theory provides the values of the electromagnetic fields in the aperture plane and beyond, the Kirchhoff vector diffraction theory (KVDT) specifies the values of fields inside the aperture plane. These already specified values can then be used to find values of the field points beyond the aperture using Green's method of solving the wave equation [2].

While the equations resulting from both these theories have to be solved using numerical methods, it is possible to derive analytical expressions for on-axis fields for both these theories. One final noteworthy point regarding these two vector diffraction theories is that for the calculations of power transferred through an aperture, the calculations made with KVDT are inaccurate for locations very near the aperture plane, as the resulting equations violate the conservation of energy principle.

The most accurate manner to predict the diffractive behavior of electromagnetic waves in a given situation is to solve Maxwell's equations using finite difference time domain (FDTD) methods. In FDTD methods, the region under consideration is discretized appropriately and the relevant equations are solved for each discrete unit. However, as FDTD methods are computationally intensive, they are mostly used for subwavelength regimes and distances close to the apertures.

3.1.3 Zone plates and diffractive lenses

A zone plate (or a Fresnel zone plate) is a diffractive optic with radially symmetrical concentric rings called zones [12]. The zones alternate between opaque and transparent. They are spaced considering the changes in path length so that light from transparent zones interferes constructively at the required focus. In a completely transparent zone plate or diffractive lens, instead of the opaque zones, there is material that introduces a variation in the optical path length, such that the phase change in the waves make them constructively interfere with the other zones at the point of focus. Generally, points in the n^{th} zone may be defined as [12],

$$\frac{(n-1)\lambda}{2} < l - l_0 < \frac{n\lambda}{2} \tag{3.6}$$

where l_0 is the optical path length from the centre of the plate to the focus, l is the distance of any other point on plate and is equal to $\sqrt{r^2 + f^2}$, λ is the wavelength and n = 1, 2, 3,... N, where N is the total number of zones. The zones with n = 1, 3, 5, … interfere constructively with the first zone, whereas n = 2, 4, 6, … interfere destructively with the first zone, but constructively with each other. So usually, the even numbered zones are covered with an appropriate absorber to maximize the interference between odd numbered zones at the focal length. A zone plate with the "reverse tone" (opaque odd numbered zones, transparent even zones) is equivalent and the effective lens will be the same. Using these equations, the external boundary of

any arbitrary zone n can be calculated for a given plane wave of wavelength λ and required focal length *f* using the following equation [12],

$$r_n^2 = n\lambda\left(f + \frac{n\lambda}{4}\right) \tag{3.7}$$

The total number of zones, N, does not affect the focal length, but it affects the resolution, efficiency and source bandwidth. The resolution, *w*, of the zone plate is approximately equal to the width of the smallest zone (which is the outermost). This approximation is accurate for the case where $f \gg \frac{n\lambda}{4}$ and the surrounding medium being air or vacuum. From this equivalence, the relations of resolution can be made with the radius of outermost zone and total number of zones [13],

$$r_n \simeq \frac{\lambda f}{2\Delta r} = \frac{\lambda f}{2w} \tag{3.8}$$

$$N = \frac{\lambda f}{4w^2} \tag{3.9}$$

3.1.4 Grating

A diffraction grating is an optical component with a periodically varying thickness or refractive index [5]. Such periodic arrangements diffract incoming waves equivalent to a number of equidistant slits of equal width [6]. The diffraction models for single and double slits can then be extended to find the intensity distribution for such arrangements. The condition for maximum intensity is the equivalent to that for the double slit (or multiple slits), but with the increasing number of slits the intensity maxima are very sharp and narrow. The intensities are therefore much higher for the grating than for a double slit. Generally, the intensity of the waves after passing through a diffraction grating is in the form of alternating minima and maxima of intensity.

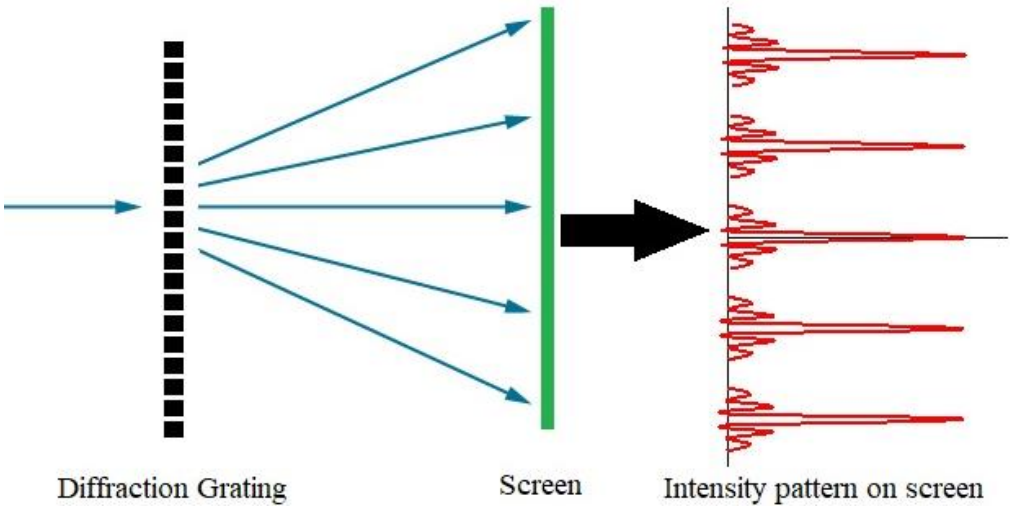

Figure 10: Cross-section view of a diffraction grating with monochromatic light

The grating equation predicts the angle θ of these maxima of intensity for a grating of slit spacing d (also known as grating period), illuminated by light of wavelength λ incident an angle i [6].

$$d \cdot \big(sin(i) + sin(\theta)\big) = m \cdot \lambda \tag{3.10}$$

Here m represents the diffraction order which has values 0, ±1, ±2, ±3 and so on. For the specific case of light being incident normal to the grating plane, the grating equation simplifies into the more common form,

$$d \cdot sin(\theta) = m \cdot \lambda \tag{3.11}$$

The property of diffraction grating that is of particular importance in spectrum splitting is the fact that the angle of diffraction is wavelength dependent. This disperses the different wavelengths of light like prisms, but unlike the refraction in prisms longer wavelengths are diffracted at larger angles, as evident from the grating equation. The dispersive nature of a grating is characterized in a quantity called angular dispersion, which is the amount of change in diffraction angle per unit change in wavelength. Mathematically [7],

$$\frac{d\lambda}{d\theta} = \frac{d}{m} \cdot \cos\theta \tag{3.12}$$

Similarly, linear dispersion at a particular distance is calculated by the following equation [7].

$$\frac{d\lambda}{dx} = \frac{d \cdot \cos\theta}{m \cdot f} \tag{3.13}$$

To separate light waves of adjacent wavelengths, the maxima of these wavelengths formed by the grating should be as narrow as possible. Mathematically, resolvance or "chromatic resolving power" is defined as [8],

$$R = \frac{\lambda}{\Delta\lambda} = m \cdot N \tag{3.14}$$

Where,

$\Delta\lambda$ = smallest resolvable wavelength difference

m = order number

N = grating frequency

The equivalence of resolvance of a grating *R* with the product of the order *m* and grating frequency *N* was determined by using the Rayleigh criterion for the diffraction maxima, i.e., two wavelengths are considered resolved when the maximum of the first lies at the minimum of the second.

Another important characteristic to consider for a grating is its profile, as the efficiency of identical gratings, under the same conditions can be different for different surface profiles [9]. Commercially available gratings are mostly either ruled gratings or holographic. Ruled gratings are fabricated by cutting periodic grooves into the substrate of the grating. Holographic gratings are formed by interference lithography in a material, usually having smoother groove surfaces with fewer defects than ruled gratings. The shapes of the grooves forming the gratings could be sinusoidal, sawtooth (triangular or trapezoidal) or lamellar profile which has rectangular ridges of fixed height and width at regular intervals [8]. Blazed gratings are a type of gratings with triangular grooves, designed to concentrate radiation into a specific diffractive order [8]. Although blazed and sinusoidal gratings can be achieved with both ruled and holographic types, ruled are more suited for blazed gratings. While sinusoidal and lamellar gratings generally offer lower peak efficiencies than a blazed grating, they usually give a broader spectral coverage [9]. For example, a 1800 g/mm sinusoidal grating's peak efficiency might be 75% for a wavelength of 400nm [10] and it would reduce rather smoothly to 50% by a 1000nm. A comparable blazed grating's peak

efficiency might be up to 95%, however it would fall off sharply and could be reduced to 35% within 200nm from its blaze wavelength [11].

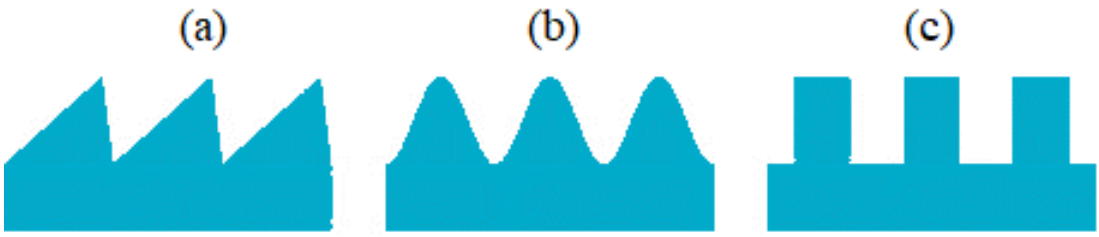

Figure 11: Types of grating by surface profile (a) Blazed (b) Sinusoidal (c) Lamellar

3.2 Discussion of design and simulation options - Ray tracing vs Physical Optics vs FDTD and their software

The class of design tools is primarily decided by the model or approximation of light that will provide the appropriate results with the computational resources available. While each model can be programmed for a required radiation and aperture patterns using programming languages (general ones such as Python or more mathematics specific like MATLAB/Octave), there are also design and simulation tools that provide users with direct access to the design functionality without the need for in-depth programming. For example, simulations of Maxwell's equations using FDTD can be run using the open source software package known as MEEP (MIT Electromagnetic Equation Propagation) or commercial tools such as Optiwave's OptiFDTD. Some tools are specific to ray-tracing or physical optics, while others such as Zemax OpticStudio, Synopsys CODE-V or Comsol Multiphysics can deal with both ray-tracing as well as physical optics models. While the finite difference time domain (FDTD) methods utilizing Maxwell equations can describe the diffraction of light even more definitively and even in cases when the other models fail, such as the sub-wavelength regime. However, it comes with much higher complexity in implementation and costs with computing resources. The design discussed here uses a diffraction grating which can be modelled with sufficient accuracy using simpler models. So, the design is carried out using the relevant equations for diffraction gratings. The widely used optical design software Zemax's trial version is used (later versions known as Zemax OpticStudio).

3.3 Design Method and Rationale

This work aimed to achieve a spectral separation system and its design methodology for splitting the solar spectrum according to a required two-junction device. Although multiple components complicate and exacerbate possible misalignments, this is simpler to design, with easier to source (possibly off-the-shelf) components. More importantly, different design parameters can be varied separately to study their effects and convert into a single element after achieving required performance.

3.3.1 Design Choices and reasoning behind them

The required spectrum splitting was obtained through the combination of two simpler, discrete elements. A diffraction grating which diffracted the incoming sunlight into different wavelength bands and a focusing lens which focused the diffracted wavelengths onto the desired PV material. The action of focusing was necessary for the separation of diffracted wavelengths at reasonable focal lengths [14]. As a side-effect, a low level of concentration was also achieved, which further improved the cell's output.

While the PV receivers were not a subject of this study their choice was necessary to guide the design of the optical system. The PV receivers were chosen from existing reported [15] cell materials, Silicon and lead-based Perovskite based on spectral response. Although the materials' spectral response curves overlap significantly their peak performance wavelengths are well separated [15].

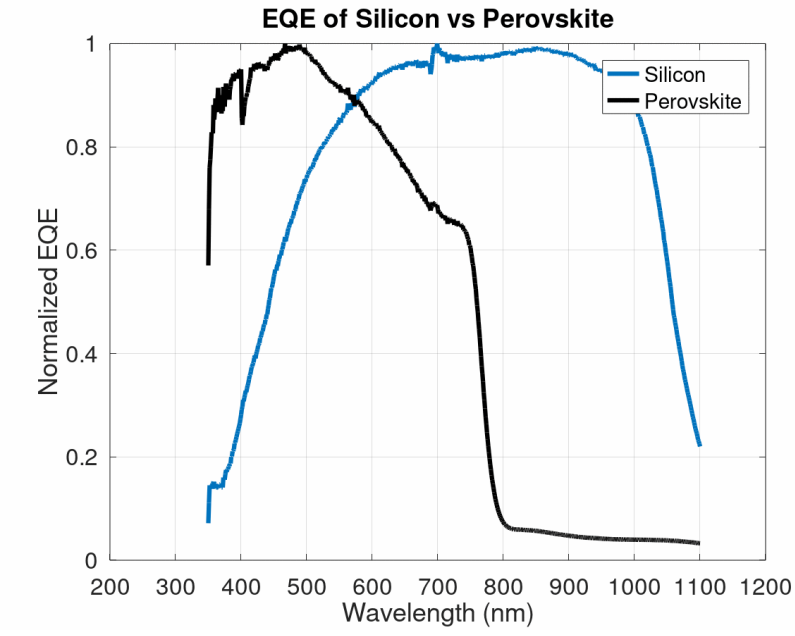

Figure 12: EQE of Silicon vs EQE of Perovskite

The choice of the cut-off wavelength (λ_c) between the two PV receivers was also crucial for the design and performance of cells. It needed to consider the facts that the spectral responses overlap, while a realistic splitting system does not possess a sharp cut-off irrespective of a range of wavelengths across an area. If chosen and/or implemented incorrectly, spectrum splitting has been shown to reduce the performance of both PV receivers and overall system [14] compared to the best bandgap material covering the entire area. Considering the chosen PV materials for the two junctions for which the selected cut-off wavelength is 570nm. This would allow the following spectrum to be utilized, instead of the standalone external quantum efficiencies shown above.

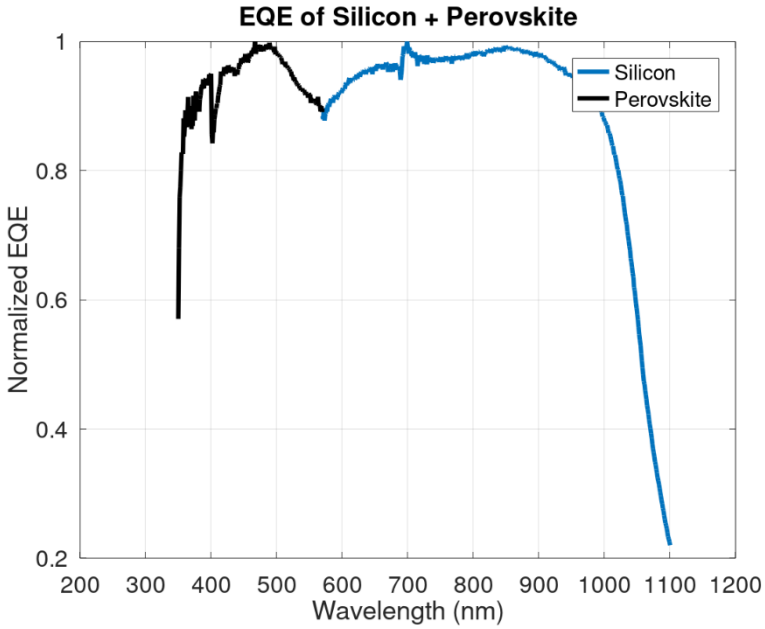

Figure 13: EQE of Silicon and Perovskite when combined at the boundary of 570nm

Two approaches can be used for the choice of the design wavelength for the system, either the cut-off wavelength can be used as the design wavelength or setting an upper limit for the boundary wavelength keeping in view of the solar spectrum and the PV receivers' responses. The off-axis angle θ has to be chosen accordingly for both cases. The first approach has control over the choice of receiver areas as well as the cut-off point, however, the behavior of longer wavelengths has to be kept in check for focusing, to avoid experiencing unintended TIR. The second approach can keep it in consideration, however, it forgoes the control over the cut-off point and the choice of receiver areas. Therefore, this design used the cut-off wavelength the design of the grating.

The grating's period was calculated by setting the targets of focal distance f and the displacement of a given wavelength over a distance *x* on the focal plane [7].

$$x = f \cdot tan\theta \tag{3.15}$$

The off-axis angle θ was calculated for diffraction at desired wavelength to achieve the targeted position of diffracted beams on the image plane. Grating period *d* was calculated from off-axis angle θ, designed wavelength λ and diffraction order (m = 1) from the grating equation 3.11. The angular and linear dispersion was calculated from equations 3.12 and 3.13.

The boundary between the two PV materials was 30 mm from the center of the optical axis and the cut-off wavelength was 570 nm (by choice) as discussed before. From these parameters, the obtained grating period *d* is 1.345 μm for a focal length of 60 mm (using (2) and (4)). The period *d* corresponded to a groove density of 740 per mm. A biconvex lens for the required focal length (60mm) was designed using the form of the lens makers' formula in eq. 3.3.

All these parameters could then be entered in the Zemax lens editor to model the required lens. However, as a lens with known performance parameters would make the performance analysis easier, a commercially available lens was chosen from the software's lens catalogue with the required focal length requirements.

3.3.2 Detail of design entered in Zemax

The summary of the system specified in Zemax is presented in Table 3:

Grating Groove Density	0.74 lines/μm
Focusing Lens Material	N-BK7
Focal length (lens)	60 mm
Radius of Curvature	60.56 mm
Thickness	8 mm
Test wavelengths	350 nm-1100 μm
Grating to lens spacing	5 mm

Table 3 Summary of system specifications in Zemax

The grating surface was given a curvature that was similar to that of the lens. A planar grating with the given groove density tended to diffract some of the longer wavelengths onto the lens at very large angles that caused them to focus at far off-axis. Furthermore, for the optimized grating period, certain wavelengths (1.25 μm-1.45 μm) were diffracted back onto the grating by a planar grating. The curvature therefore, ensures

that at least half the rays of these specific wavelengths were transmitted onwards to the lens, whereas the planar grating cut all of them off. Despite being an imported model, the lens' parameters in the software can still be customized to achieve different performance. It may also be noted that the results illustrated below are for diffraction order m = 1. This means that to achieve these results experimentally the grating is to be a blazed one (which maximizes diffraction efficiency into the particular order at which it is designed).

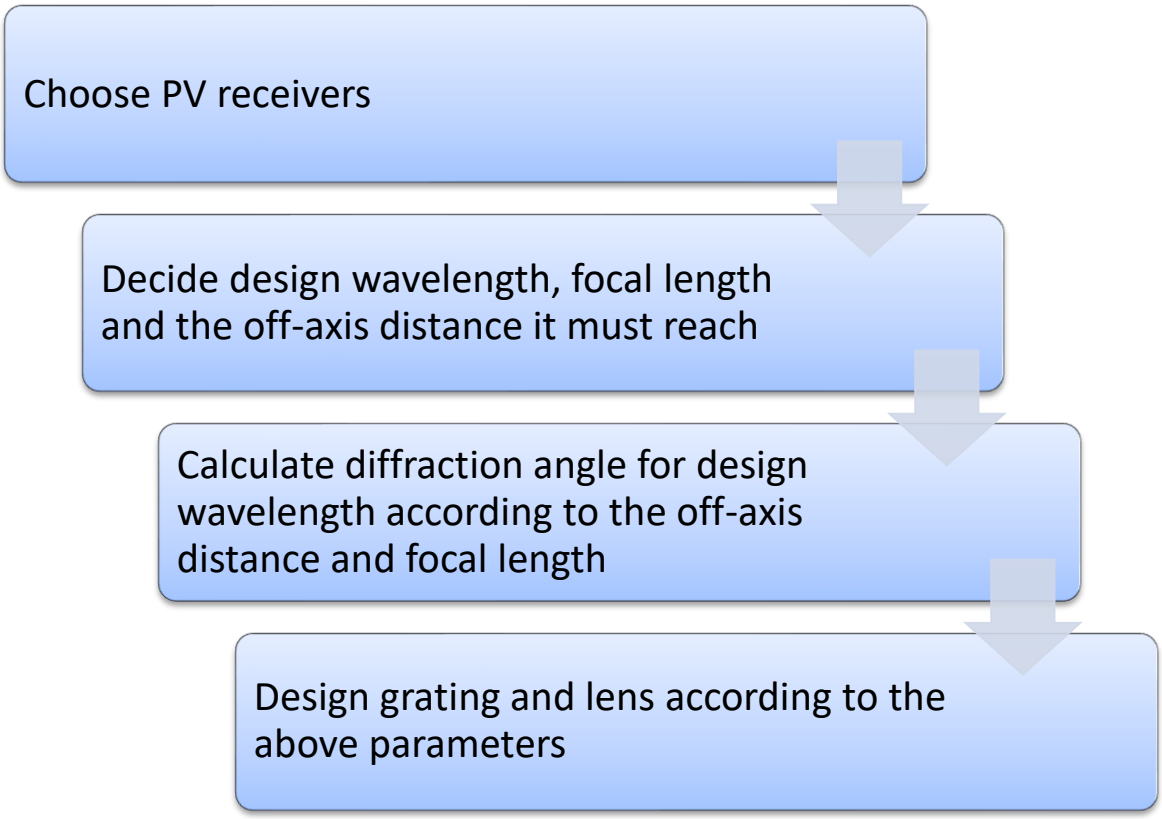

Figure 14: Overview of Design Methodology

3.4 SUMMARY

This chapter first briefly reviewed the theoretical background and mathematical formulations necessary for the target design. This review consisted of discussions on the lens makers' equation, a very brief look at the different theories of diffraction and two major diffractive components, the diffraction grating and zone plate.

Next, the software packages for design and simulation were compared based on their capabilities and requirements and Zemax OpticStudio was chosen for this study.

Having laid down the theoretical foundation and decided on the computational tools, the actual design methodology for a double junction cell was established and then utilized to come up with a design for a Silicon Perovskite double junction PV cell.

3.5 REFERENCES

[1] J. E. Greivenkamp, *Field guide to geometrical optics*. Bellingham, Washington: SPIE Press, 2004.

[2] G. D. Gillen, K. Gillen, and S. Guha, *Light Propagation in Linear Optical Media*. CRC Press, 2014.

[3] J. Peatross and M. J. Ware, *Physics of light and optics*. 2015 Ed., Brigham Young University, Provo, Utah. [Online]. Available: https://optics.byu.edu/BYUOpticsBook_2015.pdf [Accessed: 11-Dec-2019]

[4] E. A. Essex, "Hertz vector potentials of electromagnetic theory," *American Journal of Physics*, vol. 45, no. 11, pp. 1099–1101, Nov. 1977.

[5] B. E. A. Saleh and M. C. Teich, *Fundamentals of Photonics*, Second Ed. John Wiley and Sons, 2007.

[6] F. A. Jenkins and H. E. White, *Fundamentals of optics*. New York, Mc Graw-Hill Primis Custom Publ., 2010.

[7] A. Scheeline, "How to Design a Spectrometer," *Applied Spectroscopy*, vol. 71, no. 10, pp. 2237–2252, Oct. 2017.

[8] Y. G. Soskind, *Field Guide to Diffractive Optics*. SPIE Press, Bellingham, Washington, 2011.

[9] C. Palmer, *Diffraction Grating Handbook*, Sixth Ed. Newport Corp., Rochester, New York, 2005.

[10] SSI Optics, "Sinusoidal Holographic Grating | Spectrum Scientific," *Spectrum Scientific, Inc.* [Online]. Available: https://www.ssioptics.com/product-category/diffraction-gratings/sinusoidal-holographic-gratings/. [Accessed: 11-Dec-2019]

[11] SSI Optics, "Blazed Holographic Grating | Spectrum Scientific," *Spectrum Scientific, Inc.* [Online]. Available: https://www.ssioptics.com/product-category/diffraction-gratings/blazed-holographic-diffraction-gratings/. [Accessed: 11-Dec-2019]

[12] Centre for X-Ray Optics, LBL, “Fresnel Zone Plate Theory,” *Lawrence Berkeley National Lab*. [Online]. Available: http://zoneplate.lbl.gov/theory. [Accessed: 11-Dec-2019].

[13] J. Kirz and D. Atwood, “Zone Plates,” *X-Ray Data Booklet*. [Online]. Available: https://xdb.lbl.gov/Section4/Sec_4-4.html. [Accessed: 11-Dec-2019].

[14] J. M. Russo, S. Vorndran, Y. Wu, and R. Kostuk, “Comparison of dispersive and non-dispersive spectrum splitting techniques for photovoltaic systems,” in *Proceedings of 2014 IEEE 40th Photovoltaic Specialist Conference (PVSC)*, Denver, CO, USA, 2014, pp. 2257–2261.

[15] EnliTech, “How to precisely measure OPV/DSSC/Perovskite solar cells?” [Online]. Available: https://www.enlitechnology.com/show/solar-cell-characteristics.htm. [Accessed: 11-Dec-2019].

CHAPTER 4: RESULTS, ANALYSIS AND DISCUSSION

4.1 RESULTS

The linear dispersion for the system was at an average of 0.02 µm/mm, which was in line with the calculations for the initial design. The focus of 30 mm off-axis was achieved at the 570 nm cut-off wavelength. The designed system layout's spot diagram illustrating the separation is shown in Fig. 15.

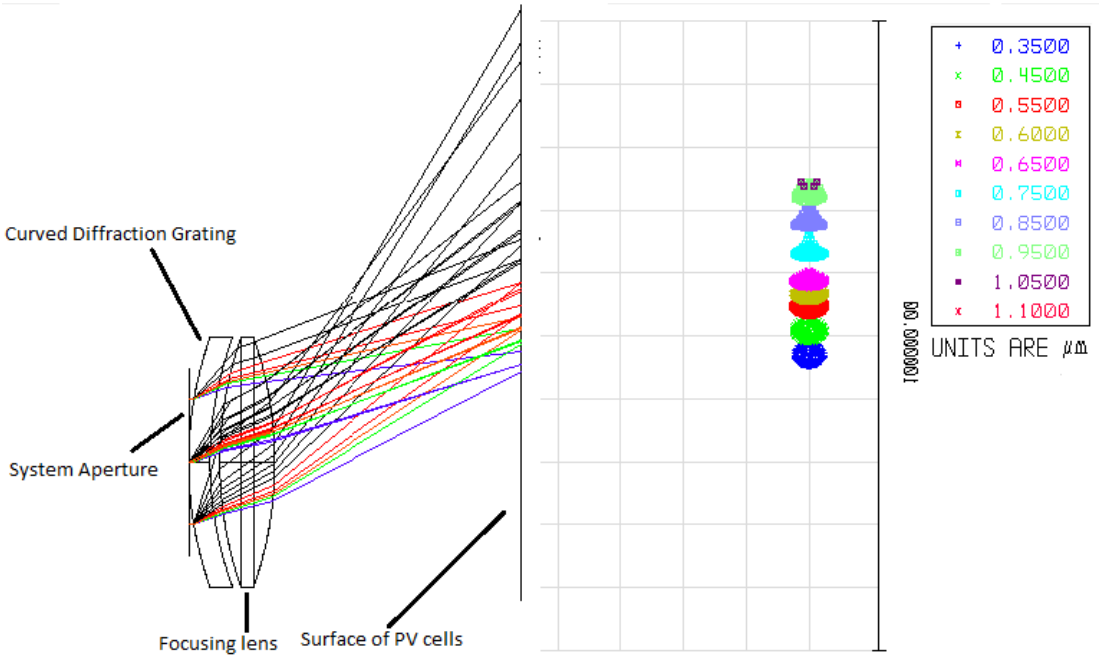

Figure 15: Resulting Layout and Spot Diagram for 3mm spacing system

This meant that the widths of the Perovskite and Silicon layers would need to be 25 mm and 15 mm, respectively for the use of spectrum tail for the device considered at 1.45 µm. Though the useful spectrum in terms the PV materials under consideration is mostly up to 1100nm and the spectrum to be used for analysis is from 350nm to 1100nm. These widths are practically achievable for manufacturing solar cells with the given PV materials.

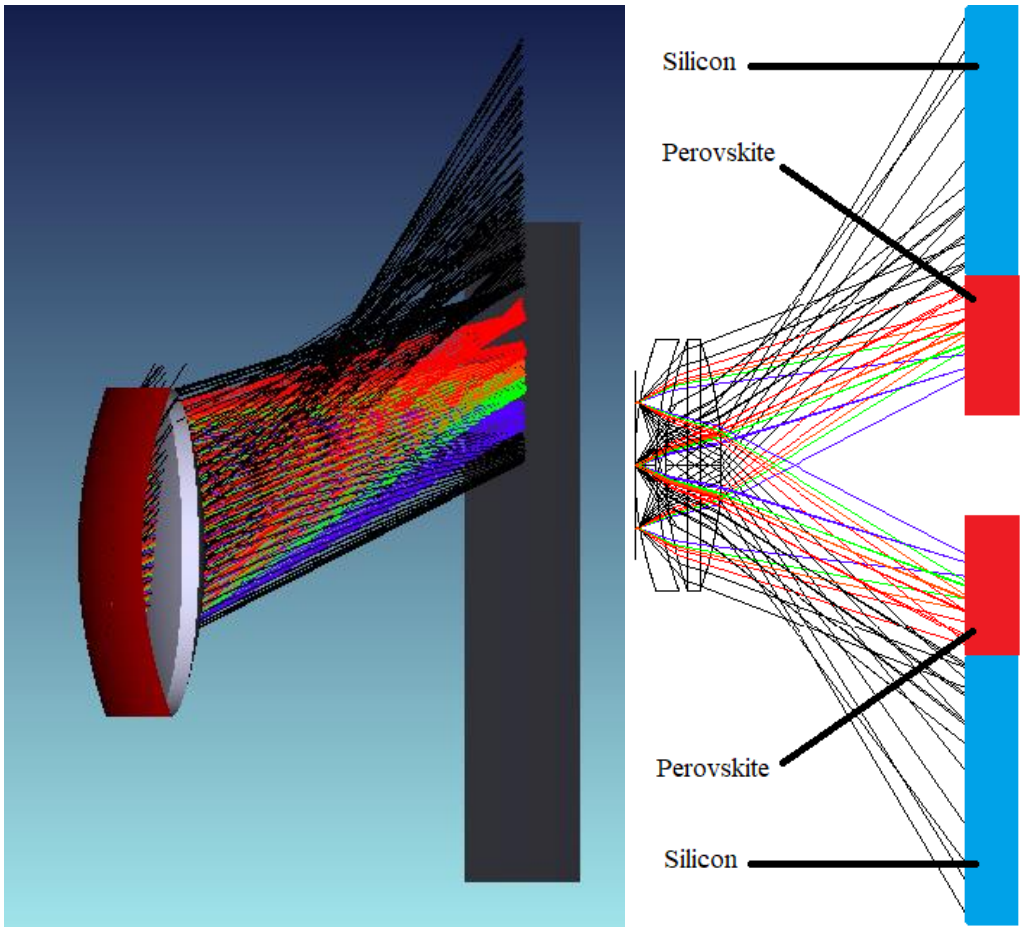

Figure 16: Shaded model and layout with approximate positions of the PV cells

4.2 ANALYSIS

An important design variable that was not explicitly determined in the preceding calculations was the distance between the grating and the focusing lens. Four different configurations were tested at 1 mm, 3 mm, 5 mm and 10mm separations as shown in Fig. 17.

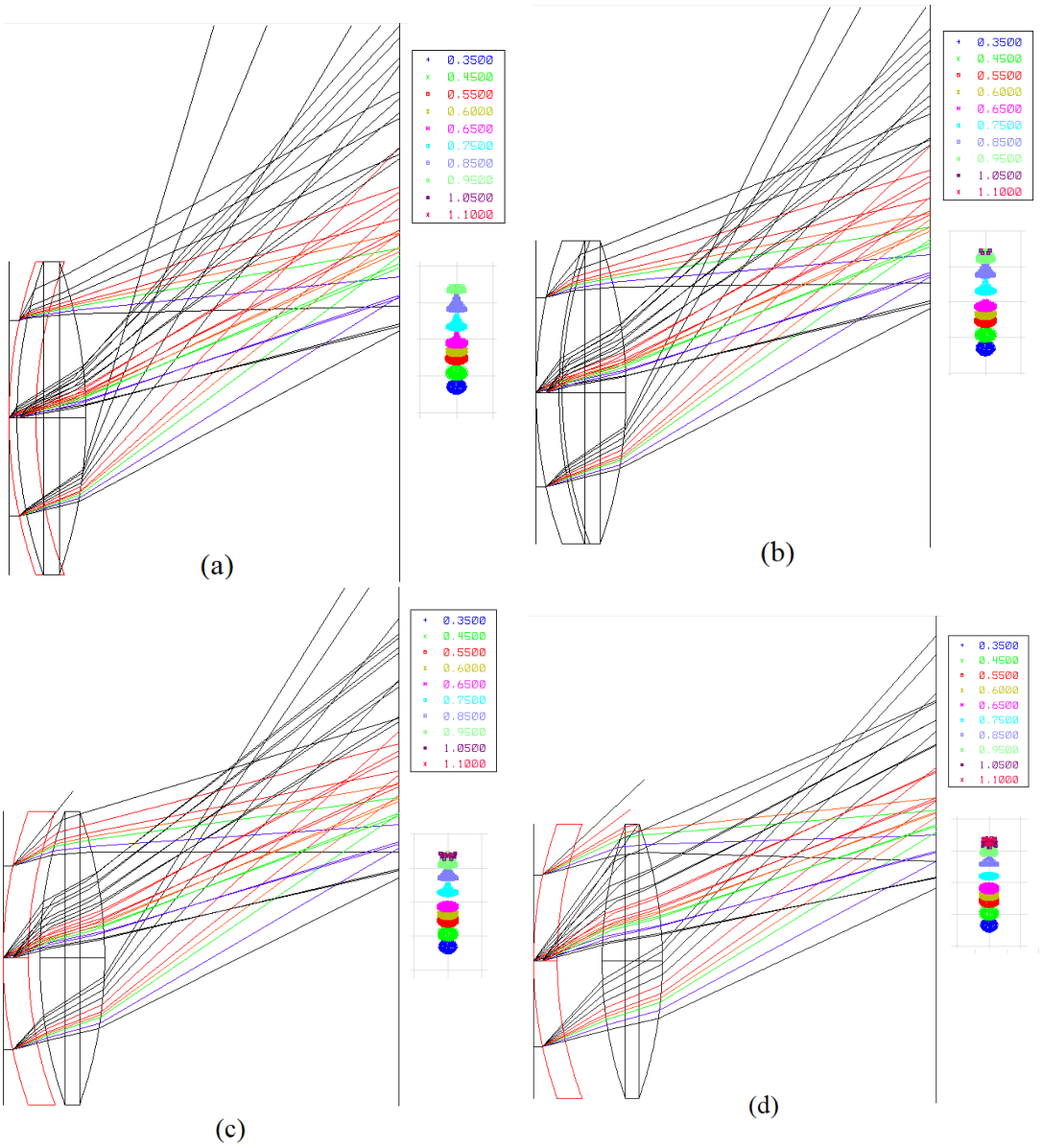

Figure 17: Four configurations according to lens-grating distance (a) 1 mm (b) 3 mm (c) 5 mm (d) 10 mm

If the two elements are too close, the device could be very compact, but it is observed that some of the wavelengths encounter the lens at angles that are not focused enough. However, if the spacing is too large some of the rays diffracted by the grating escaped the system in the gap without passing through the lens. The distance of 3 mm was found to be the adequate balance between a compact design and yields performance at the fixed optimized values of the rest of design variables.

Considering the spot diagrams for each configuration, the difference in spectral separation for the band of interest was negligible for our application, though the off-axis distances and foci were being affected.

4.2.1 Photocurrent calculation and comparison

The primary performance metric chosen to judge the design methodology proposed here was the photocurrent. The photocurrent from individual cells was compared to the photocurrent from the overall system designed here.

The major components in the path of light and the manner in which they affected the light reaching the cells was as follows,

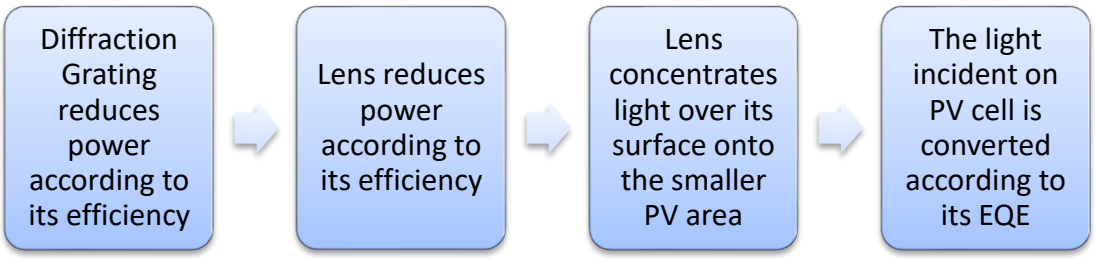

Figure 18: Sequence of phenomena that alter the solar irradiance in the system

The grating significantly reduces power, depending on a number of factors discussed in the grating section in the previous chapter. For this design, it is assumed that a sinusoidal grating is in effect. As the efficiency curve is flatter, for the simplicity of calculation this allowed an average value for the grating efficiency to be calculated for the spectrum of interest, which flatly affects all wavelengths across the spectrum. The lens (material NBK-7) also reduces power, though this is almost flatly across most of the spectrum and the effect is very small [1]. Concentration increases the power per unit area incident on the PV material according to concentration ratio. Finally, the amount of power of each wavelength was converted to electricity (represented by the EQE).

The photocurrent (or more accurately, photocurrent density), J_L can be calculated from a given spectrum and external quantum efficiency using the following equation [2],

$$J_L = -q.\int E(\lambda).\frac{\lambda}{h.c}.EQE(\lambda)d\lambda \qquad (4.1)$$

Here, the terms "$E(\lambda).\frac{\lambda}{h.c}$" denote the irradiance $E(\lambda)$ being divided by the energy of an individual photon ($\frac{h.c}{\lambda}$) at that wavelength and it gives the number of photons for

that wavelength. Multiplying this by $EQE(\lambda)$ gives the number of those photons that successfully gave an electron. Integrating that over all the wavelengths of interest yields the total number of electrons and finally the multiplication by electronics charge q gives the actual current density.

As the spectrum is being manipulated in in this system, the $E(\lambda)$ term in the equation is going to be the ASTM G-173 AM1.5 solar spectrum modified according to the spectrum splitting system. The above integral could be solved for given conditions using numerical methods such as the Simpson's rule. However, the EQE data available for both receivers and the irradiance is with a resolution of 1 nm and the irradiance data in the ASTM G-173 standard is $Wm^{-2}.nm^{-1}$ instead of W/m2.nm.str. This allows the simplification of the integral equation into the following discrete summation,

$$J_L = \sum E(\lambda).\frac{\lambda}{h.c}.EQE(\lambda) \tag{4.2}$$

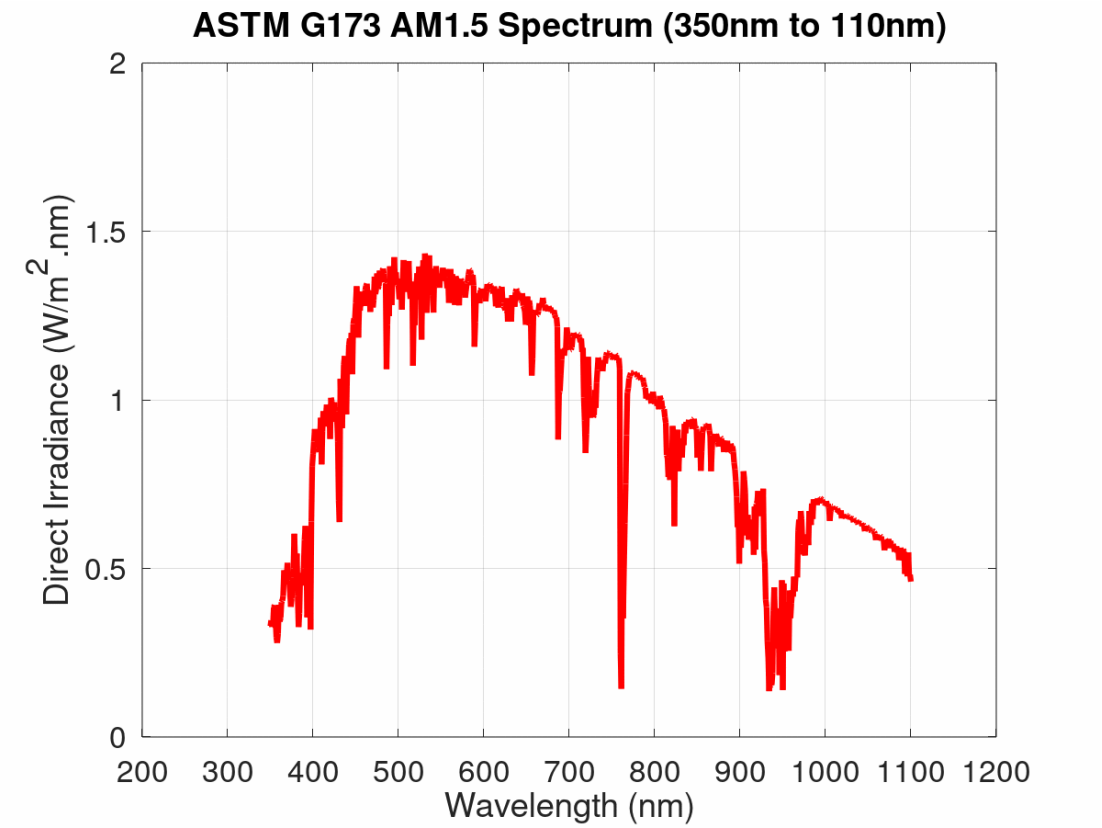

Figure 19: ASTM G-173 AM1.5 Spectrum

The tool used for mathematical simulations in this analysis was GNU Octave, which is an open source alternative to MATLAB. Octave and MATLAB's syntaxes are mostly compatible, save for some toolkit and function names.

In Octave the above equation 4.2 was simulated for both PV receivers separately in their own wavelength ranges. For simulation, the ASTM G-173 data was loaded according to the range and resolution of the EQE data available (from 350 to 1100nm range, steps of 1nm, using the direct irradiance only. The EQE data was provided by Wisnu Ananda and its measurement is detailed in [3].

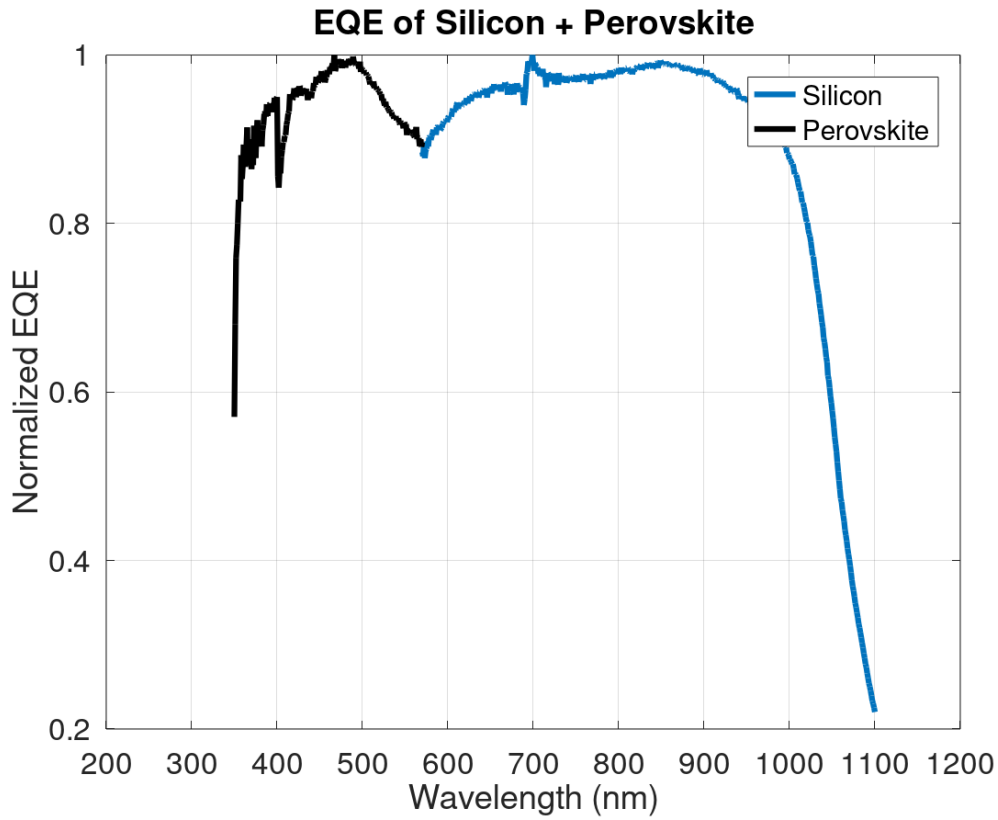

Figure 20: Combined EQE of Silicon and Perovskite that is used by the system

The power from solar irradiance was reduced according to the grating (~65% efficiency) and lens effects (BK-7 transmissivity ~95% for the band in question). Both these effects are assumed flatly across all wavelengths under consideration. (It should be noted that polarization (especially S-polarization aka TM waves) affects the efficiency of gratings but was not considered in this calculation). Furthermore, the energy divided among orders is not considered in this calculation. A sinusoidal grating which maximizes power in the +1 and -1 orders would be consistent with these assumptions when the underlying cells are arranged accordingly. Finally, the power

received from the previous steps was multiplied according to the concentration factors, which was calculated according to the Zemax results. For each PV receiver area by dividing the area of the lens over the area of each PV receiver.

$$C_{geo,P} = \frac{\pi.(12.5mm)^2}{6mm \cdot 15mm} = 5.46 \quad (4.3)$$

$$C_{geo,Si} = \frac{\pi.(12.5mm)^2}{6mm \cdot 25mm} = 3.27 \quad (4.4)$$

The irradiance $E(\lambda)$ (modified according to concentration and efficiency calculations) is obtained for use in eq. 4.2.

During the calculation in GNU Octave using eq. 4.2, each wavelength λ was converted into metres during the calculation, where q was the elementary charge, h was Planck's constant and c is the speed of light. Only λ was variable and changed with each new value of EQE (λ) and E(λ). The EQE for each corresponding wavelength was extracted from the standards' initial file and saved in a separate CSV file for ease of loading into Octave.

These calculations were made separately for the Perovskite (I_{LP} from 350nm to 600nm) and Silicon (I_{LS} 600nm to 1100nm). For the total photocurrent density I_L, the two were added.

For comparison, the photocurrent density was also calculated for Silicon and Perovskite cells separately, using the exact wavelength ranges and data as above, without the effects of optical systems. Using the above methodology, the following results were obtained, (values in $\frac{mA}{cm^2}$)

$$I_L = 84.999$$

For comparison,

Silicon photocurrent calculated without any of the optical manipulation using the same data,

$$I_{LSi0} = 32.625$$

Perovskite photocurrent calculated without optical manipulation using the same data,

$$I_{LP0} = 18.768$$

System Output Parameter	Value
Photocurrent density, I_L	84.99 $\frac{mA}{cm^2}$
Concentration Ratio over Silicon, $C_{geo,Si}$	3.27
Concentration Ratio over Perovskite, $C_{geo,P}$	5.46
Linear Dispersion, $\frac{d\lambda}{dx}$	0.02 μm/mm
Total Throw (System), TOTR	51.8mm

Table 4: Summary of important system output parameters

4.3 DISCUSSION

4.3.1 Comparison with literature

As evident from the results of the optical simulations and the calculations made in the light of those calculations, the combined effect of the concentration and splitting resulted in a significant increase in the photocurrent density (I_L = 84.999 $\frac{mA}{cm^2}$) when compared to the standalone photocurrents of Si and Perovskite (I_{LSi0} = 32.625 $\frac{mA}{cm^2}$ and I_{LP0} = 18.768 $\frac{mA}{cm^2}$ respectively) calculated for the same irradiance and EQE data using the same method. Also, a significant spectral separation of 0.02 μm/mm was achieved within a total throw of 51.8mm, despite the fact that the system used more than one component. This clearly demonstrates the compactness that can be achieved with diffractive optical elements when compared to refractive systems such as [4], which had a focus 36cm away and 23cm off-axis. When compared to other diffraction-based designs such as [5] [6], the total throw of the system is less than or comparable to the focal lengths of 75mm and 50cm, despite the fact that the other designs used single diffractive elements. But this comes at a cost of concentration ratios (3.27 for Silicon and 5.46 for Perovskite in our case), which was lower than the other two junction devices [5] [6]. Though the focus of this design was optimal separation and concentration wasn't explicitly considered during the design process.

While there are certain adjustments that need to be made before the results in this text can be compared rigorously with the results from similar designs in literature, the optical efficiency of 61.25% of the current design was found to be comparable to the figures discussed earlier in chapter, marginally higher than some but lower than others.

The photocurrent density of the design presented here they still gives a good idea regarding the performance of the system. Even if it is assumed that there is no change in voltage, the enhancement in photocurrent is ~2.5 times the performance without the spectral management and concentration. The improvement can be mostly attributed to better separation as a result of the decoupling of diffraction from focusing function and different PV receiver choices, other factors such receiver sizes, tolerance to misalignment, polarization sensitivity and some smaller factors are not considered in this analysis.

The better concentration ratios and more optimized, variable spaced grating reported in literature would probably perform better, however they required customized components which increase the cost and time to test, which are two advantages that the current design exhibits and is discussed ahead.

4.3.2 Significance and Utility of the design methodology

Another significant aspect of this work is the design methodology used here. It can be used to design a spectrum splitting system for any combination of a lateral, two junction photovoltaic cell. The straight forward methodology can be used to quickly design a prototype, spectrum separation system to test a given combination of cells in an experimental setting. This is also aided by the fact that the design tries to use as many off-the-shelf optical components as possible. This would allow lesser use of custom-made optical elements and more use of commercial mass-produced components. This would result in quicker prototyping at lower costs. Furthermore, the designs can be used to study the effects of different parameters of the system separately, to better understand the interplay of diffraction, focusing, distances within the system, angles of incidence and off-axis angles etc.

Applications of the design methodology and the designed system outside the lab and experimentation would be limited to area where higher power at smaller area and weight is more important than the extra cost incurred by the use of these optical elements. This mostly occurs in space-based applications such as satellites. Another unintended advantage of space is that the solar spectrum is mostly direct above the atmosphere. And the optical system makes use of direct solar irradiance.

4.4 SUMMARY

This chapter analysed and discussed the design methodology as well as the resulting design in its various configurations. The design was analysed primarily based on the spectral separation it achieved and the enhancement in photocurrent due to the splitting and concentration of sunlight. The effects of the different components in the path of sunlight on the efficiency of the system were discussed for the photocurrent calculations and the equations used for photocurrent calculation were discussed in detail. Using the photocurrent equation, solar irradiance data from ASTM and EQE data for Silicon and Perovskite, the photocurrent resulting from the designed system was calculated and compared to the same calculations for bare Silicon and Perovskite cells. It was found that there was significant enhancement in the photocurrent. The results were then discussed in the background of the results from other designs reviewed in chapter 2. Finally, the significance of the design methodology was discussed for various practical applications as well as experimentation in multijunction photovoltaics.

4.5 REFERENCES

[1] Präzisions Glas & Optik, "N-BK7 | Optical borosilicate-crown glass from SCHOTT | BK 7." [Online]. Available: https://www.pgo-online.com/intl/BK7.html. [Accessed: 12-Dec-2019].

[2] K. Jager, O. Isabella, R. van Swaaij, A. H.M. Smets, and M. Zaman, *Solar Energy - Fundamentals, Technology, and Systems*. First Ed. Delft University of Technology, Netherlands, 2014.

[3] W. Ananda, "External quantum efficiency measurement of solar cell," in *Proceedings of 2017 15th International Conference on Quality in Research (QiR): International Symposium on Electrical and Computer Engineering*, Nusa Dua, Indonesia, pp. 450–456, 2017.

[4] M. Stefancich, A. Zayan, M. Chiesa, S. Rampino, L. Kimerling, and J. Michel, "Single element spectral splitting solar concentrator for multiple cells CPV system," *Optics Express*, vol. 20, no. 8, pp. 9004-9018, 2012.

[5] A. Albarazanchi, P. Gerard, P. Ambs, and P. Meyrueis, "Design of single layer subwavelength diffractive optical element (G-Fresnel) for spectrum splitting and beam concentration," *Proceedings of SPIE 9131, Optical Modelling and Design III*, Brussels, Belgium, p. 913126, May 2014.

[6] C. Michel, J. Loicq, F. Languy, and S. Habraken, "Optical study of a solar concentrator for space applications based on a diffractive/refractive optical combination," *Solar Energy Materials and Solar Cells*, vol. 120, pp. 183–190, Jan. 2014.

CHAPTER 5: CONCLUSION AND FUTURE WORK

5.1 CONCLUSION

A two-junction, diffractive spectrum splitting system was designed and evaluated using simulations, in the light of literature, optics theory and available data. Its performance was judged primarily by calculating the photocurrent density and it showed great performance improvements when compared to the same PV cells without optical manipulation. The performance comparison against other two junction, diffractive spectrum splitting system gave mixed results. Considering increase in output power, system compactness and robustness, the designed system exceeded some designs in some areas while others in other areas. The utility of the design methodology was identified in prototyping spectrum splitting systems and checking various combinations of PV cells. The particular design was found to be more useful in some special cases such as small scale, space-based PV systems. It was also observed that the design and analysis methods could be further improved from various aspects, which would result in better designs that are more accurately characterized by the analysis method, before they manufactured or assembled.

5.2 POSSIBLE AREAS OF IMPROVEMENT AND FUTURE WORK

There are numerous areas where the design and analysis methods used here could be improved. Firstly, the current design methodology considers the focusing lens only for improved separation of the different wavelengths and the achieved geometric concentration is only a positive side effect. If the methodology can be modified to optimize the concentration ratio in addition to the separation, the power output can be greatly increased within the same number of optical elements. Another possible improvement would be to incorporate the distance between grating and the focusing lens into the design calculations. This could be possible if a quantified relation is obtained between this length and the optical performance parameters such as optical efficiency and dispersion of the overall system. Furthermore, the possible use of subwavelength gratings and the advantages and disadvantages they would bring need to be considered as part of the overall design procedure, to further enhance the options

available during design. As grating types change the diffraction efficiencies considerably across wavelengths and polarizations, it is also worth investigating how the different grating types fit into the design methodology and how the design methodology might have to be modified for different grating types.

Another important consideration for efficiency is the effect of temperature, as the concentration of sunlight is involved. While the concentration ratios are low and spectrum splitting means the cells do not heat up as much as they would without splitting, the effect of temperature on photocurrent would need to be considered in a more complete analysis for even more realistic photocurrent figures. This is particularly important for Perovskite, for which not only the current would be affected, but also the stability of the material.

Another point to consider is the mismatch between the foci of the different wavelengths and the length to PV receivers. As the wavelengths focus over a curved surface, ideal separation and concentration ratios cannot be achieved when the PV receivers are assumed to be planar. And as it is practically more feasible to have planar PV cells, the obvious area to target is the design of the grating to focus the various wavelengths in the same plane. One possibility is the use of variable spaced gratings, though that means customized production and would mean that some of the methodology advantages mentioned above would have to be forsaken.

Lastly, to make this methodology more useful, it would also be fruitful to study how this two-component design can be translated into a single diffractive optical element. Not just a trial and error method to achieve a system that has the same performance, but a mathematically and physically consistent procedure that can convert any design from this methodology into a single diffractive optical lens.

Now considering the analysis of the design in the previous section of this chapter, the first and obvious improvement would be to calculate the power conversion efficiency of the device for better performance characterization. This would require obtaining the data regarding the voltage and power output of the cells for which the EQE and spectral responsivity was used. Another possible addition to the analysis process would be the determination of the exact efficiency of the grating under consideration for the wavelengths of interest. This would give more accurate figures for the optical efficiency. Similarly, by considering the effects of different polarizations of light and

how they are affected throughout the optical path in the system would improve the efficiency calculations, as polarization is affects diffraction efficiency, especially in the subwavelength regime. This would become necessary if the subwavelength gratings are made part of the design process.

Design of a Diffractive Spectrum Splitting System for Lateral Multijunction Photovoltaics using Ray Tracing

Behlol Nawaz
US-Pakistan Centre for Advanced Studies in Energy (USPCAS-E)
National University of Science and Technology (NUST)
Islamabad, Pakistan.
behlolnawaz@outlook.com

Muhammad Rizwan Saleem
Institute of Photonics
University of Eastern Finland
Joensuu, Finland.
US-Pakistan Centre for Advanced Studies in Energy (USPCAS-E)
National University of Science and Technology (NUST)
Islamabad, Pakistan.

Nadia Shahzad
US-Pakistan Centre for Advanced Studies in Energy (USPCAS-E)
National University of Science and Technology (NUST)
Islamabad, Pakistan.

***Abstract*—Solar power has the potential to fulfill a significant part of global energy needs and avoid the issues with conventional energy sources. Within solar power technologies, photovoltaics (PV) offer many advantages, but the efficiency of its single junction variant is limited by the Shockley-Queisser limit and stacked multi-junction (MJ) cells have their own manufacturing and economic hurdles. Spectrum splitting techniques have the potential to overcome these challenges for MJ cells and provide high efficiency panels, at a reasonable cost, for large scale use. This paper explores the design methodology of a solar spectrum splitting system, aiming to design a compact, diffraction-based light splitter for a given set of laterally arranged solar cells. A two-component spectrum splitting and concentration system is designed with a curved grating and focusing lens, for a two junction, Perovskite/Silicon cell combination, which achieves a reasonable separation between the wavelength bands for the two cells.**

Keywords - spectrum splitting; photovoltaics; multijunction; diffractive, solar;

I. INTRODUCTION

Renewable energy sources have the potential to avoid the serious issues with conventional sources, such as impact on climate change [1] and limited reserves. Solar power is one of the frontrunners in terms of raw potential among alternative energy sources. Among the solar power technologies, photovoltaics (PV) (conversion of sunlight directly into electricity) have received a lot of attention in terms of research activities as well as overall adoption [2]. However, for photovoltaic (PV) technologies to be feasible and competitive against non-renewables on a truly global scale, they must become more cost-effective. One of the possibilities to achieve this is the improvement of power conversion efficiency (PCE), which results in a smaller area requirement for PV panels, reducing the cost of panel materials and number of panels, as well as the real estate required for their deployment.

The efficiency of single junction PV devices are limited to the "Shockley-Queisser limit" [3], which is 30 % for a 1.1 eV bandgap device considered with an approximation to the solar spectrum (blackbody radiation at 6000 K). According to more recent studies using the now standard AM 1.5 spectrum, this could be up to 33.7 % for an ideal 1.34 eV bandgap device [4]. Single junction devices are slowly approaching this limit (up to 29.1 % without concentration [5]). There might be possible slight significant improvement in the future i.e., more efforts would probably be aimed at making the high efficiency variants devices which are commercially feasible.

One approach to side step around the Shockley-Queisser limit is to use multiple (PV) materials in a cell, better known as tandem solar cells or multijunction solar cells [6]. The concept of multijunction cells is to have multiple PV conversion materials (such as Silicon, GaAs, CIGS, Perovskite etc.), with each material type converting a spectral range close to its bandgap's energy, so a higher fraction of the solar spectrum can be converted more efficiently. This is because a single junction can only convert the wavelengths of light with energy above its bandgap (so lower energy bandgaps are not converted at all) and the energy in excess of the bandgap energy is wasted as thermal energy.

There are two major approaches to multijunction solar cells. One is often referred to as the stacked or monolithic multijunction (Fig. 1(a)), which consists of different PV material layers of increasing bandgap stacked one on top of the other towards the illuminated radiation [6]. Each layer absorbs and converts its relevant wavelengths, while the rest continue onwards to the lower layers. The second approach is to split the spectrum of solar radiation into different bands before it reaches the PV material (Fig. 1(b)), with each band reaching its appropriate PV receiver.

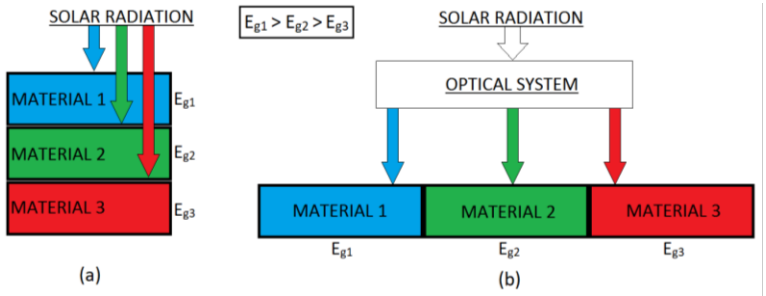

Figure 1 – (a) Stacked and (b) Laterally arranged spectrum splitting for PV

II. BACKGROUND AND DESIGN CONSIDERATIONS

Most of the current record holding cells are vertically stacked multijunctions under concentrated sunlight. [5] On the other hand, PV layers are often arranged "laterally", though

other geometries are also used to generate similar effects [7,8] i.e., the spectrum splits by optical manipulation before reaching to the spectrally designed PV receiver. Lateral multijunctions with spectrum splitting have some potential advantages such as,

a. No lattice matching requirements between PV materials [6], which results in,
   i. Easier and possibly cost-effective manufacturing
   ii. Relatively fewer challenges to the choice of materials owing to lattice matching
b. No constraints on current flow and no need of tunnel junctions [6]
c. Slower degradation and enhancement in operating life. Each cell only absorbs a portion of the solar spectrum, they experience lower operational temperatures which decreases their rate of degradation [9]

However, they require methods for accurate and efficient splitting of the incoming solar spectrum onto the PV absorbers in the cells. There are numerous methods to split the spectrum for PV, [6,10], they are often loosely classified into being Selective Reflection/Transmission [8,11], refraction [12,13], luminescence [14,15] or diffraction [16–19] (all illustrated in Fig. 2) and combination [7,20] based systems.

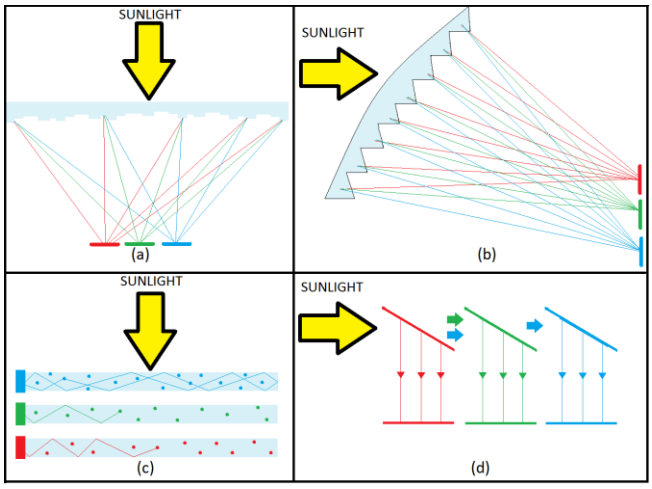

Figure 2 – Categories of Solar Spectrum Splitting Techniques (a) Diffraction (b)Luminescence (c)Selective Transmission (d)Refraction. The figure visualizes each PV receiver with the colour of its respective wavelength

This study focuses on the design of a diffraction-based system. The primary reason for choosing diffraction-based elements for this design is that diffractive optical elements (DOEs) are compact and their operation is compatible with planar cell geometries [9]. Furthermore, a diffractive element can combine splitting and focusing into the same element (called Spectrum Splitting Beam Concentration, SSBC) efficiently. [22]

Several approaches have been used in recent years to design diffraction-based spectrum splitting systems for multijunction PV cells. These include a diffraction grating superimposed on the surface profile of a Fresnel lens (single sided G-Fresnel, Fig. 3(a)) [18,22,25], combinations of diffraction grating and Fresnel lens on separate sides of an optical element, (double sided G-Fresnel, Fig. 3(b)) [9,23,24] and various configurations of holographic elements [8,16,17]. Gratings have also been used in combination with total internal reflection (TIR) [20].

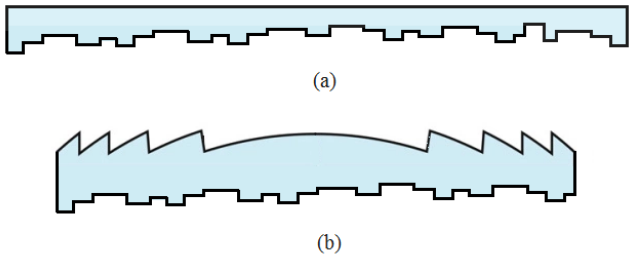

Figure 3 – Cross-sections of (a) Single-Sided G-Fresnel (b) Double-Sided G-Fresnel. One surface carries out both functions (splitting and concentration) in a single-sided G-Fresnel, while both surfaces in a double-sided G-Fresnel split and focus separately.

Holographic optical elements have been reported to achieve remarkable efficiencies [16] and are well suited to combining the spectrum splitting and focusing functions in a single element. However, the instability of holography materials (such as dichromated gelatin, DCG) is a serious challenge [26] and an active area of research. Single-sided G-Fresnel might be easier to integrate over lateral MJ cells (as one side can be flat), but their surface profiles are complicated to design as well as manufacture. This can result in higher costs and lower efficiency due to imperfections in the final product. While the surface profiles of both sides of a double-sided G-Fresnel are important to the operation of the system, they are still compact and easier to design.

Therefore, this study discusses part of a design methodology which eventually aims at achieving a double-sided G-Fresnel.

III. Design Methodology

A. *Overall methodology*

This work aims to achieve a design of spectral separation of illuminated solar spectrum by using multiple optical components. Although multiple components complicate and exacerbate possible misalignments, this is simple to design, with easier to source (possibly off-the-shelf) components and therefore would make validation of a design easier to achieve. More importantly, different design parameters can be varied separately to study their effects and convert into a single element after achieving required performance.

B. *Choice of Design and Analysis Tools*

The class of design tools is primarily decided by the model or approximation of light that will provide the appropriate results with computational resources in study. In general, diffraction is considered as a part of physical optics and is modeled with either the Fraunhofer or Fresnel equations considering light as waves [27]. However, a specific case of diffraction grating can also be visualized in terms of rays using the grating equation [27]. The finite difference time domain

(FDTD) methods utilizing Maxwell equations can describe the diffraction of light even more definitively in most cases. Even when the other models fail, such as the sub-wavelength regime. However, it comes with much higher complexity in implementation and costs with computing resources.

The current target design utilizes optical elements that can be described by ray-tracing with sufficient accuracy. So, the design is carried out using the relevant equations. There are several optical design packages that can be used for such a design. The widely used optical design software Zemax's trial version is used (later versions known as Zemax OpticStudio).

C. Design

The required spectrum splitting is obtained through the combination of two simpler, discrete elements. A diffraction grating which diffracts the incoming sunlight into different wavelength bands and a focusing lens which focuses the diffracted wavelengths onto the desired PV material. The focusing is important for separating diffracted wavelengths at shorter focal lengths [28] and also to achieve a low level of concentration to improve the cell's output.

The splitting system is designed for a two-junction device. While the PV receivers are not a subject of this study their choice is necessary to guide the design of the optical system. The PV receivers are chosen from existing reported [29] cell materials, Silicon and lead-based Perovskite based on spectral response. The materials' spectral response curves overlap significantly which are less in comparison to other common material combinations and their peak performance wavelengths are well separated [29].

The choice of the cut-off wavelength (λ_c) between the two PV receivers is also crucial for the design and performance of cells. It needs to consider the facts that the spectral responses overlap and a realistic splitting system will not possess a sharp cut-off irrespective of a range of wavelengths across an area. If chosen and/or implemented incorrectly, spectrum splitting has been shown to reduce the performance of both PV receivers and overall system [28] compared to the best bandgap material covering the entire area. Considering the chosen PV materials for the two junctions for which the selected cut-off wavelength is 600nm.

Two approaches can be used for the choice of the design wavelength, either the cut-off wavelength can be used as the design wavelength or setting an upper limit for the boundary wavelength keeping in view of the solar spectrum and the PV receivers' responses. The off-axis angle θ has to be chosen accordingly for both cases. The first approach has control over the choice of receiver areas as well as the cut-off point, however, the behavior of longer wavelengths has to be kept in account (for focusing) to avoid experiencing unintended TIR. The second approach can keep it in evaluation, however, it forgoes the control over the cut-off point and the choice of receiver areas. Here, the cut-off wavelength is used for the design of the grating.

The grating's period is calculated by setting the targets of focal distance f and the displacement of a given wavelength over a distance x on the focal plane [30].

$$x = f \cdot \tan\theta \tag{1}$$

The off-axis angle θ can be calculated for diffraction at desired wavelength to achieve the targeted position of diffracted beams on the image plane. Grating period d is calculated from off-axis angle θ, designed wavelength λ and diffraction order ($m = 1$) from grating equation [30].

$$d \cdot \sin\theta = m \cdot \lambda \tag{2}$$

The angular and linear dispersion is calculated from the following equations [30]:

$$\frac{d\lambda}{d\theta} = \frac{d}{m} \cdot \cos\theta \tag{3}$$

$$\frac{d\lambda}{dx} = \frac{d \cdot \cos\theta}{m \cdot f} \tag{4}$$

The boundary between the two PV materials is 30 mm from the center of the optical axis and the cut-off wavelength is 600 nm. From these optimized engineering parameters, the obtained grating period d is 1.345 µm for a focal length of 60 mm (using (2) and (4)). The period d corresponds to a groove density of 740 per mm.

A biconvex lens for the required focal length (60mm) can be designed using the following form of the lens makers' formula, [27]

$$\frac{1}{f} = (n-1) \cdot \left[\frac{1}{R_1} - \frac{1}{R_2} + \frac{(n-1) \cdot d}{nR_1R_2}\right] \tag{5}$$

where R_1 and R_2 are radii of curvature of the two surfaces of the lens, n is the refractive index of the material of the lens and d is the distance between them. All these parameters can then be entered in the Zemax lens editor to model the required lens. However, as a lens with known performance parameters will make the performance analysis easier, a commercially available lens is chosen from the software's lens catalog with the required focal length.

D. Design Entry in Zemax

The system is specified in Zemax with the following parameters:

Table 1 - Design parameters for the system

Grating Groove Density	0.74 lines/µm
Focusing Lens Material	N-BK7
Focal length (lens)	60 mm
Radius of Curvature	60.56 mm
Thickness	8 mm
Test wavelengths	350 nm-1450 µm
Grating to lens spacing	5 mm

The grating surface is given curvature that is similar to that of the lens. A planar grating with the given groove density tends to diffract some of the longer wavelengths onto the lens at very large angles that causes to focus at far off-axis. Furthermore, for the optimized grating period, certain wavelengths (1.25 μm-1.45 μm) are diffracted back onto the grating by a planar grating. The curvature therefore, ensures that at least half the rays of these specific wavelengths are transmitted onwards to the lens, whereas the planar grating cut all of them off. Despite being an imported model, the lens' parameters in the software can still be customized to achieve different performance. It may be noted that the results illustrated below are for diffraction order $m = 1$. This means that to achieve these results experimentally the grating is to be a blazed one (which maximizes diffraction efficiency into the particular order at which it is designed). The design layout is given in Fig. 4.

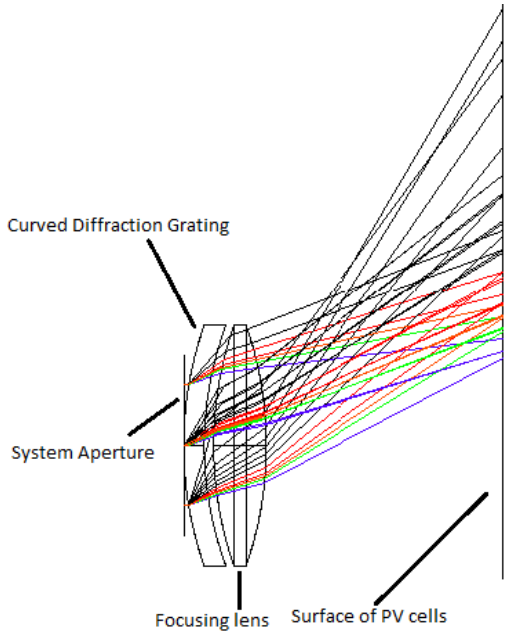

Figure 4 – Layout with 5mm spacing between grating and lens. The first curved structure from the left is a diffraction grating whereas the second is the focusing lens

IV. Results and Analysis

The achieved linear dispersion is obtained at an average of 0.02 μm/mm, which is in line with the calculations for the initial design, using (4). The focus of 30 mm off-axis was achieved at 600 nm cut-off wavelength. The achieved system layout's spot diagram illustrating the separation is shown in Fig. 5.

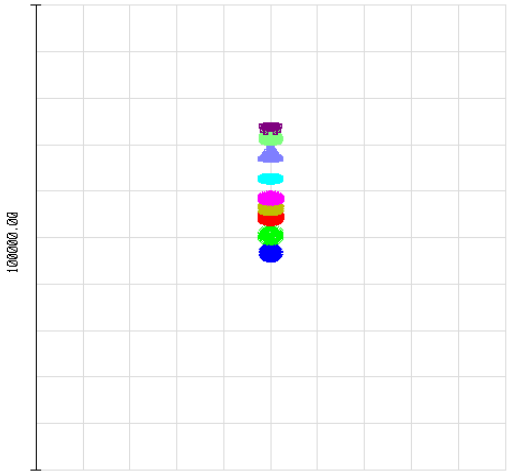

Figure 5 - Spot Diagram on the image plane (PV cell) in the XY axes, showing separation of wavelengths from 350 to 1050 nm along the Y-axis. Units in micrometers.

This meant that the widths of the Perovskite and Silicon layers would need to be 30 mm and 47 mm, respectively for the use of spectrum tail for the device considered at 1.95 μm. (A local minimum in power in the AM1.5 spectrum, the following maximum of which is near 0.1 W/m^2). These widths are practically achievable for manufacturing solar cells with the given PV materials.

An optimized design considers a significant variable that was not explicitly determined in the preceding calculations, which is the distance between the grating and the focusing lens. Three different configurations are tested at 1 mm, 10 mm and 5mm separations as shown in Fig. 6(a), (b) and (c) respectively.

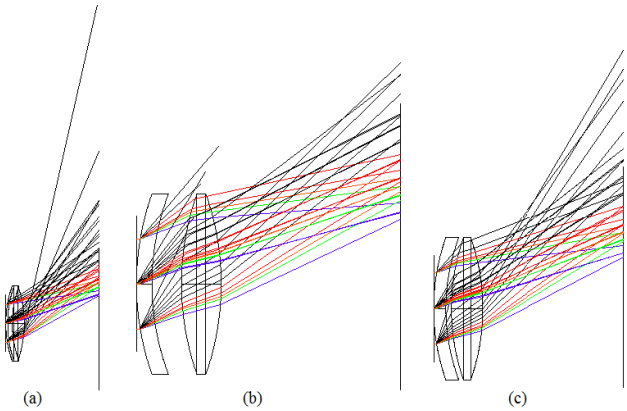

Figure 6 – The three different configurations with repect to the grating/lens distance. (a) 1mm (b) 10mm (c) 5mm

If the two elements are too close, the device could be very compact, but it is observed that some of the wavelengths encounter the lens at angles that are not focused enough. However, if the spacing is too large some of the rays diffracted by the grating escaped the system in the gap without passing through the lens. 5 mm is found to be the

adequate balance between a compact design and yields performance at the fixed optimized values of the rest of design variables.

V. Conclusion and Outlook

The design of a multi-component, diffractive, spectrum splitting system utilizing a diffraction grating and a biconvex lens is carried out. A linear dispersion of 0.02 μm/mm is achieved at an effective focal length of 53.8 mm from the aperture. The rationale behind the choice of the design wavelength for the diffraction grating is discussed. Curvature is introduced in the surface of the diffraction grating, which can cater to some of the issues present in the use of the planar grating. The effect of the distance between the grating and the lens is also briefly discussed. A reasonable separation is obtained between the target wavelength bands and the PV receiver areas of the designed system are 30 mm and 47 mm respectively, which can be manufactured practically. Furthermore, the design process can be used to come up with a spectrum splitting system to any combination of PV cells.
This is the first part of a design process which can be further used for a double-sided G-Fresnel design. In addition to the process of converting this design to the desired target, calculations regarding PCE, concentration ratios and the effects of different geometries within the different design parameters may be explored for their effects on the performance.

References

[1] Stocker, T.F., D. Qin, G.-K. Plattner, M. Tignor, S.K. Allen, J. Boschung, A. Nauels, Y. Xia, V. Bex and P.M. Midgley (eds.) “IPCC, 2013: Climate Change 2013: The Physical Science Basis. Contribution of Working Group I to the Fifth Assessment Report of the Intergovernmental Panel on Climate Change”. Cambridge University Press, Cambridge, United Kingdom and New York, NY, USA, 1535 pp, 2013

[2] Michael Schmela, “Report: Global Market Outlook 2018-2022", Solar Power Europe, 27th June 2018.

[3] William Shockley, J. Hans Queisser, “Detailed Balance Limit of Efficiency of p-n Junction Solar Cells”, Journal of Applied Physics, Vol. 32, Issue 3, pp 510-519, 1961.

[4] Sven Rühle, “Tabulated values of the Shockley–Queisser limit for single junction solar cells”, Solar Energy, Volume 130, pp 139-147, 2016.

[5] MA Green, Y Hishikawa, ED Dunlop, Dean H. Levi, Jochen Hohl-Ebinger, Masahiro Yoshita, Anita W.Y. Ho-Baillie, “Solar cell efficiency tables (Version 53)”, Progress in Photovoltaics: Research and Applications, Vol. 27, Issue 1, pp 3-12, 2019.

[6] A.G. Imenes, D.R. Mills, “Spectral beam splitting technology for increased conversion efficiency in solar concentrating systems: a review,” Solar Energy Materials and Solar Cells, Volume 84, Issues 1–4, Pages 19-69, 2004.

[7] P. Blain, C. Michel, L. Clermont, F. Languy, M. Décultot, S. Habraken, C. Lenaerts, K. Fleury-Frenette, D. Vandormael and J. Loicq, “Spectral splitting planar solar concentrator: Experimental testing of a design aiming at dye sensitized solar cells,” Proc. of SPIE Vol. 9140, Photonics for Solar Energy Systems V, 2014.

[8] Silvana Ayala P., Shelby Vorndran, Yuechen Wu, Benjamin Chrysler, Raymond Kostuk, “Segmented Holographic Spectrum Splitting Concentrator,” Next Generation Technologies for Solar Energy Conversion VII, Proc. of SPIE Vol. 9937, 2016.

[9] Céline Michel, Jérôme Loicq, Tanguy Thibert, and Serge Habraken, “Optical study of a spectrum splitting solar concentrator based on a combination of a diffraction grating and a Fresnel lens,” AIP Conference Proceedings 1679, 070002, 2015.

[10] Ahmad Mojiri, Robert Taylor, Elizabeth Thomsen, Gary Rosengarten, “Spectral beam splitting for efficient conversion of solar energy—A review”, Renewable and Sustainable Energy Reviews, Volume 28, Pages 654-663, 2013.

[11] Hisashi Uzu, Mitsuru Ichikawa, Masashi Hino, Kunihiro Nakano, Tomomi Meguro, José Luis Hernández, Hui- Seon Kim, Nam-Gyu Park, and Kenji Yamamoto, “High efficiency solar cells combining a perovskite and a silicon heterojunction solar cells via an optical splitting system,” Applied Physics Letters 106, 013506, 2015.

[12] Carlo Maragliano, Matteo Chiesa and Marco Stefancich, “Point-focus spectral splitting solar concentrator for multiple cells concentrating photovoltaic system,” Journal of Optics, Volume 17, 105901, Number 10, 2015.

[13] Carlo Maragliano, Harry Apostoleris, Matteo Bronzoni, Stefano Rampino, Marco Stefancich, and Matteo Chiesa, "Efficiency enhancement in two-cell CIGS photovoltaic system with low-cost optical spectral splitter," Opt. Express 24, A222-A233, 2016.

[14] Kaifeng Wu, Hongbo Li, Victor I. Klimov, “Tandem luminescent solar concentrators based on engineered quantum dots”, Nature Photonics, Volume 12, Issue 2, p.105-110, 2018

[15] Francesco Meinardi, Samantha Ehrenberg, Lorena Dhamo, Francesco Carulli, Michele Mauri, Francesco Bruni, Roberto Simonutti, Uwe Kortshagen and Sergio Brovelli, “Highly efficient luminescent solar concentrators based on earth-abundant indirect-bandgap silicon quantum dots” Nature Photonics, Volume 11, Issue 3, 177-185, 2017.

[16] Yuechen Wu, Benjamin D. Chrysler, Raymond K. Kostuk, "Design and fabrication of cascaded dichromate gelatin holographic filters for spectrum-splitting PV systems," Journal of Photonics for Energy 8(1), 017001, 2018.

[17] Yuechen Wu, Raymond K. Kostuk, "Two-junction holographic spectrum-splitting micro-concentrating photovoltaic system," Journal of Photonics for Energy, SPIE, Vol. 7, 017001, 2017.

[18] Jia Li, Wen-Qi Xu, Jia-Sheng Ye, Peng Han, Wen-Feng Sun, Sheng-Fei Feng, Xin-Ke Wang, Yan Zhang, “High focusing efficiency or high signal-to-noise ratio diffractive optical element for color separation and light focusing,” Optik, Volume 138, Pages 87-94, 2017.

[19] Benjamin D. Chrysler, Yuechen Wu, Zhengshan Yu, Raymond K. Kostuk, “Volume holographic lens spectrum-splitting photovoltaic system for high energy yield with direct and diffuse solar illumination,” Next Generation Technologies for Solar Energy Conversion VIII, Proceedings of SPIE Vol. 10368, 103680G, 2017.

[20] Céline Michel, Pascal Blain, Lionel Clermont, Fabian Languy, Cédric Lenaerts, Karl Fleury-Frenette, Marc Décultot, Serge Habraken, Denis Vandormael, Rudi Cloots, Gopala Krishna V.V. Thalluri, Catherine Henrist, Pierre Colson, Jérôme Loicq, “Waveguide solar concentrator design with spectrally separated light”, Solar Energy, Volume 157, Pages 1005-1016, 2017.

[21] Cameron Stanley, Ahmad Mojiri and Gary Rosengarten, "Spectral light management for solar energy conversion systems," Nanophotonics, Vol. 5, Issue 1, Pages 161-179, 2016.

[22] Abbas Albarazanchi, Philippe Gérard, Pierre Ambs, Patrick Meyrueis, Giang-Nam Nguyen, and Kevin Heggarty, "Smart multifunction diffractive lens experimental validation for future PV cell applications," Optics Express, 24, A139-A145, 2016.

[23] Celine Michel, Jerome Loicq, Tanguy Thibert, Serge Habraken, "Optical Study of diffraction grating/Fresnel lens combinations applied to a spectral-splitting solar concentrator for space applications", Applied Optics, Vol. 54, No. 22, Pages 6666-6673, 2015.

[24] Celine Michel, Jerome Loicq, Fabian Languy, Serge Harbraken, "Optical study of a solar concentrator for space applications based on

a diffractive/refractive optical combination", Solar Energy Materials and Solar Cells, Volume 120, Part A, Pages 183-190, 2014.

[25] Wen-Qi Xu, Dong-Feng Lin, Xin Xu, Jia-Sheng Ye, Xin-Ke Wang, Sheng-Fei Feng, Wen-Feng Sun, Peng Han, Yan Zhang, Qing-Bo Meng and Guo-Zhen Yang, "Simple and universal method in designs of high-efficiency diffractive optical elements for spectrum separation and beam concentration", Chinese Phys. B Vol 26, No. 7, 074202, 2017.

[26] Benjamin Chrysler, Silvana Ayala Pelaez, Yuechen Wu, Shelby Vorndran, Raymond Kostuk, "Environmental stability study of holographic solar spectrum splitting materials," Next Generation Technologies for Solar Energy Conversion VII, Proc. of SPIE Vol. 9937, 2016.

[27] Francis Jenkins, Harvey White, "Fundamentals of Optics," 4th Ed. McGraw-Hill.

[28] Juan M. Russo, Shelby Vorndran, Yuechen Wu, Raymond Kostuk, "Comparison of Dispersive and Non-Dispersive Spectrum Splitting Techniques for Photovoltaic Systems", IEEE 40th Photovoltaic Specialist Conference (PVSC), Denver, CO, pp. 2257-2261, 2014.

[29] EnliTech, *How to precisely measure OPV /DSSC/Perovskite Solar cells?* [online] Available at https://www.enlitechnology.com/show/solar-cell-characteristics.htm [Accessed 3 Apr 2019].

[30] Alexander Scheeline, "How to Design a Spectrometer." *Applied Spectroscopy*, Vol. 71, No. 10, 2237–52 (October 2017).

//Not published at the time of printing of this thesis

Design and Analysis of a Diffractive Spectrum Splitting System for a Silicon-Perovskite Double Junction Solar Cell

Behlol Nawaz[1, a)], Nadia Shahzad[1, b)], Wisnu Ananda[2] and Muhammad Rizwan Saleem[1, 3]

[1]*US-Pakistan Center for Advanced Studies in Energy (USPCAS-E), National University of Science and Technology (NUST), Islamabad, Pakistan.*
[2] *Center for Material and Technical Product (B4T), Ministry of Industry, Indonesia*
[3] *Institute of Photonics, University of Eastern Finland, Joensuu, Finland*

[a)] Corresponding author: behlolnawaz@outlook.com
[b)] nadia.shahzad@uspcase.nust.edu.pk

Abstract. The efficiency of single junction photovoltaic (PV) cells is limited to the Shockley-Queisser limit. Multijunction is one of the most commonly studied concepts for working around this limit, but multijunctions with each layer stacked on top of the other have specific fabrication and financial hurdles. Spectrum splitting methods can potentially avoid these challenges to make the widespread use of multijunction cells more feasible. This paper explores a method for the design of a compact diffractive splitting system that distributes the solar radiation between laterally arranged Silicon and Perovskite PV cells. The two-component system splits the 350nm to 1100nm band into two bands of 350-570nm and 570-1100nm for Perovskite and Silicon respectively, while simultaneously achieving low concentration levels. The photocurrent density is calculated using experimental external quantum efficiency (EQE) data along with the split and concentrated spectrum and it is found that the photocurrent is enhanced by ~2.5 times by the optical manipulation.

INTRODUCTION

Sustainable energy sources have the potential to cater to a significant part of the world's energy requirements while avoiding the problems with conventional sources such as limitations of reserves and detrimental effects on the environment. [1] Compared to the other solar power technologies, photovoltaics (PV) (direct conversion of sunlight to electric power) has been more popular in general adoption as well as research efforts. [2] Photovoltaic (PV) technologies can be more feasible and competitive against non-renewables on a much greater scale, if they can become more cost-effective. One possible way of achieving this is the enhancement of power conversion efficiency (PCE), so that smaller areas of PV panels can produce more power, reducing the cost of panel materials and number of panels, as well as the real estate required for their deployment.

The efficiency limit for single junction PV devices is known as the "Shockley-Queisser limit" [3] and it is 30 % for a 1.1 eV bandgap device, when considered with an approximation to the solar spectrum (blackbody radiation at 6000 K). More recent studies using the now standard ASTM AM 1.5 spectrum put this number up to 33.7 % for an ideal 1.34 eV bandgap device [4]. Single junction devices are gradually increasing their efficiencies and approaching this limit (up to 29.1 % without concentration [5]).

One method often studied for circumventing the Shockley-Queisser limit is to use multiple p-n junctions (or multijunctions) in a cell [6]. The concept of multijunction cells is based on the fact that a single junction can only convert the wavelengths of light with energy above its bandgap, so lower energy bandgaps are not converted at all and the energy in excess of the bandgap energy is wasted as thermal energy. With multiple junctions of various

materials with different bandgaps, each junction can convert its relevant wavelengths more efficiently, thereby increasing the overall efficiency.

The arrangement of multijunctions in a cell can be classified into two major categories. One is often referred to as the stacked or monolithic multijunction (Fig. 1(a)), which consists of different PV material layers of increasing bandgap stacked one on top of the other towards the illuminated radiation [6]. Each layer absorbs relevant wavelengths, while the rest continue onwards to the lower layers. The second approach is to split the spectrum of solar radiation into different bands before it reaches the PV material (Fig. 1(b)), with each band reaching its appropriate PV receiver.

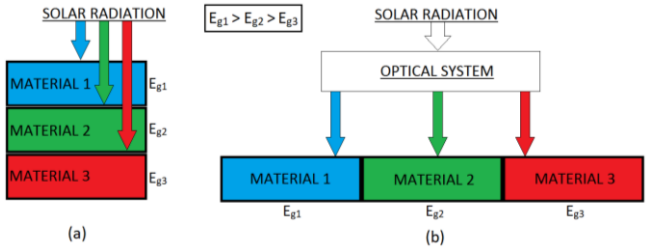

Figure 1 – (a) Stacked and (b) Laterally arranged spectrum splitting for PV

Stacked multijunctions (under concentrated sunlight) hold most of the current records for conversion efficiencies. [5] On the other hand, the alternate, spectrum splitting approach which usually uses laterally arranged cells (though other geometries are also used to generate similar effects), [7,8] have some potential advantages such as,

a. No need for lattice matching between PV materials [6], which results in,
   i. Easier and possibly cost-effective manufacturing
   ii. Relatively fewer limits on the choice of materials
b. No constraints on current flow and no need of tunnel junctions [6]
c. Slower degradation which potentially increases the operational life of the cell. This is mainly because each junction only absorbs a specific part of the solar spectrum, so the overall heating is reduced. [9]

There are various methods to split the spectrum for PV, [6,10], which can be classified into being Selective Reflection/Transmission [8,11], refraction [12,13], luminescence [14,15] or diffraction. [16–19] Some designs use combinations [7,20] of these methods.

The focus of this study is to design a diffraction-based system. Diffraction was chosen considering the fact that diffractive optical elements (DOEs) are compact and their operation is compatible with planar cell geometries [9]. Furthermore, a diffractive element can easily combine splitting and focusing into the same element efficiently (called Spectrum Splitting Beam Concentration, SSBC). [22]

Diffractive spectrum splitting systems explored in recent literature include diffraction gratings superimposed on the surfaces profile of Fresnel lenses (called single sided G-Fresnel, Fig. 3(a)) [18,22,25], combinations of diffraction grating and Fresnel lens on separate sides of an optical element, (double sided G-Fresnel, Fig. 3(b)) [9,23,24] and various configurations of holographic elements [8,16,17]. Gratings have also been used in combination with total internal reflection (TIR) [20].

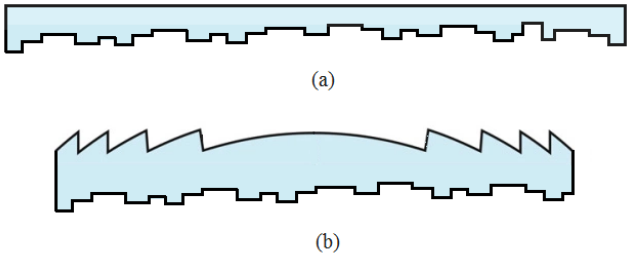

Figure 2 – Cross-sections of (a) Single-Sided G-Fresnel (b) Double-Sided G-Fresnel. One surface carries out both functions (splitting and concentration) in a single-sided G-Fresnel, while both surfaces in a double-sided G-Fresnel split and focus separately.

Spectrum splitting with holographic optical elements have been reported to achieve remarkable efficiencies [16] and are well suited to combining the spectrum splitting and focusing functions in a single element. However, the instability of holography materials (such as dichromated gelatin, DCG) is a serious challenge. [26] The surface profiles of single-sided G-Fresnels are complicated to design as well as manufacture. This can result in higher costs and lower efficiency due to imperfections in the final product. While two different surface profiles have to be catered to in the design of a double-sided G-Fresnel, they are still compact and easier to design.

METHODOLOGY

This work takes a simpler approach which aimed at achieving splitting of the solar spectrum by using multiple optical components. Although multiple components complicate alignment and increase the possibilities of misalignments, it was simpler to design, with easier to source (close to off-the-shelf) components with known properties and therefore made the validation of a design easier to achieve. More importantly, different design parameters were varied separately to study their effects and could be converted into a single element after achieving required performance.

Design

The required spectrum splitting was obtained through the combination of a diffraction grating which diffracted the incoming sunlight (with varying diffraction angles according to wavelength) and a lens which focused the diffracted wavelengths onto the desired PV cell. The focusing was important for separating diffracted wavelengths at shorter focal lengths [28] and also provided a low level of concentration to improve the cell's output.

The splitting system was designed for a two-junction device. While the PV receivers themselves were not a subject of this study, their choice was necessary to guide the design of the optical system. Silicon and lead-based Perovskite were chosen because while their spectral response curves overlapped, the overlap was lesser in comparison to other combinations and their peak performance wavelengths are well separated.

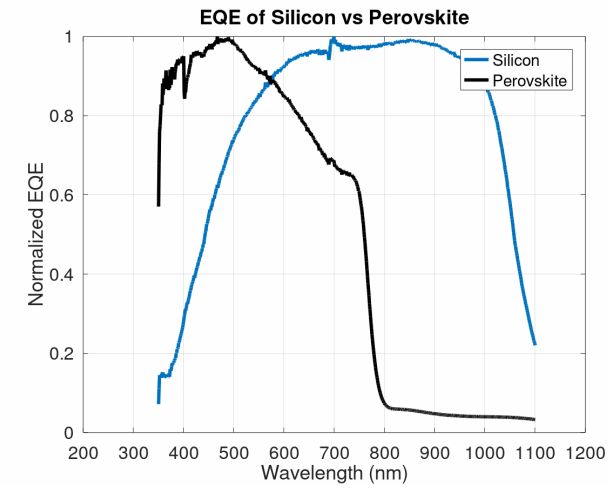

Figure 3 - EQE of Silicon vs EQE of Perovskite

The choice of the cut-off wavelength (λ_c) between the two PV receivers was also crucial for the design and performance of cells. In addition to the spectral response curves, it needed to consider the fact that a realistic splitting system will not possess a sharp cut-off irrespective of a range of wavelengths across an area. If chosen and/or implemented incorrectly, spectrum splitting has been shown to reduce the performance of both PV receivers and the overall system. [28] compared to the best bandgap material covering the entire area. Considering the EQE data available for Silicon and Perovskite, the cut-off wavelength was set at 570nm.

Next, two approaches could have been used for the choice of the design wavelength, either the cut-off wavelength between the two receivers or an upper limit for the boundary wavelength keeping in view the solar spectrum and the PV receivers' responses. The off-axis angle θ then had to be chosen accordingly for both cases. The first approach had control over the choice of receiver areas as well as the cut-off point, however, the behavior of longer wavelengths has to be kept in account (for focusing) to avoid experiencing unintended TIR. The second approach can keep it in evaluation, however, it forgoes the control over the cut-off point and the choice of receiver areas. Here, the cut-off wavelength was used for the design of the grating.

The grating's period was calculated by setting the targets of focal distance *f* and the displacement of a given wavelength over a distance *x* on the focal plane [29].

$$x = f \times tan\theta \tag{1}$$

The off-axis angle θ was calculated for diffraction at the desired wavelength to achieve the targeted position of diffracted beams on the image plane. Grating period *d* was then calculated from off-axis angle θ, designed wavelength λ and diffraction order (*m = 1*) from the simpler version of the grating equation [29].

$$d \cdot \sin\theta = m \cdot \lambda \tag{2}$$

The angular and linear dispersion was calculated from the following equations [29]:

$$\frac{d\lambda}{d\theta} = \frac{d}{m} \cdot \cos\theta \tag{3}$$

$$\frac{d\lambda}{dx} = \frac{d \cdot \cos\theta}{m \cdot f} \tag{4}$$

The boundary between the two PV materials was set at 30 mm from the center of the optical axis and the cut-off wavelength was 570 nm. From these parameters, the obtained grating period *d* was 1.345 µm for a focal length of 60 mm (using (2) and (4)). The period *d* corresponded to a groove density of 740 per mm.

A biconvex lens for the required focal length (60mm) was designed using the following form of the lens makers' formula, [27]

$$\frac{1}{f} = (n-1) \cdot \left[\frac{1}{R_1} - \frac{1}{R_2} + \frac{(n-1) \cdot d}{nR_1R_2}\right] \tag{5}$$

where R_1 and R_2 are radii of curvature of the two surfaces of the lens, *n* is the refractive index of the material of the lens and *d* is the distance between them. All these parameters were then entered in the Zemax lens editor to model the required lens. However, as a lens with known performance parameters made the performance analysis easier, a commercially available lens was chosen from the software's lens catalog with the required focal length.

The system was specified in Zemax with the following parameters:

Table 1 - Design parameters for the system

Grating Groove Density	0.74 lines/µm
Focusing Lens Material	N-BK7
Focal length (lens)	60 mm
Radius of Curvature	60.56 mm
Thickness	8 mm
Test wavelengths	350 nm-1100 µm
Grating to lens spacing	3 mm

A planar grating with the given groove density tended to diffract some of the longer wavelengths onto the lens at angles that caused them to focus at far off-axis, while some wavelengths at the edge of the grating were diffracted sharply and missed the lens entirely. The grating surface was then given curvature similar to that of the lens. It may be noted that the results illustrated below are for diffraction order *m* = 1. This means that to achieve these results experimentally, the grating has to maximize power in the ±1 diffraction orders.

//Not published at the time of printing of this thesis

RESULTS AND ANALYSIS

Results

The linear dispersion for the system was at an average of 0.02 μm/mm, which was in line with the calculations for the initial design. The focus of 30 mm off-axis was achieved at the 570 nm cut-off wavelength. The designed system layout's spot diagram illustrating the separation is shown in Fig. 5(b) below.
This meant that the widths of the Perovskite and Silicon layers would need to be 25 mm and 15 mm, respectively for the use of spectrum tail for the device considered at 1.45 μm. Though the useful spectrum in terms the PV materials under consideration is mostly up to 1100nm and the spectrum to be used for analysis is from 350nm to 1100nm. These widths are practically achievable for manufacturing solar cells with the given PV materials.

Analysis

An important design variable that was not explicitly determined in the preceding calculations was the distance between the grating and the focusing lens. Four different configurations were tested at 1 mm, 3 mm, 5 mm and 10mm separations as shown in Fig. 5 (a), (b), (c) and (d) respectively.

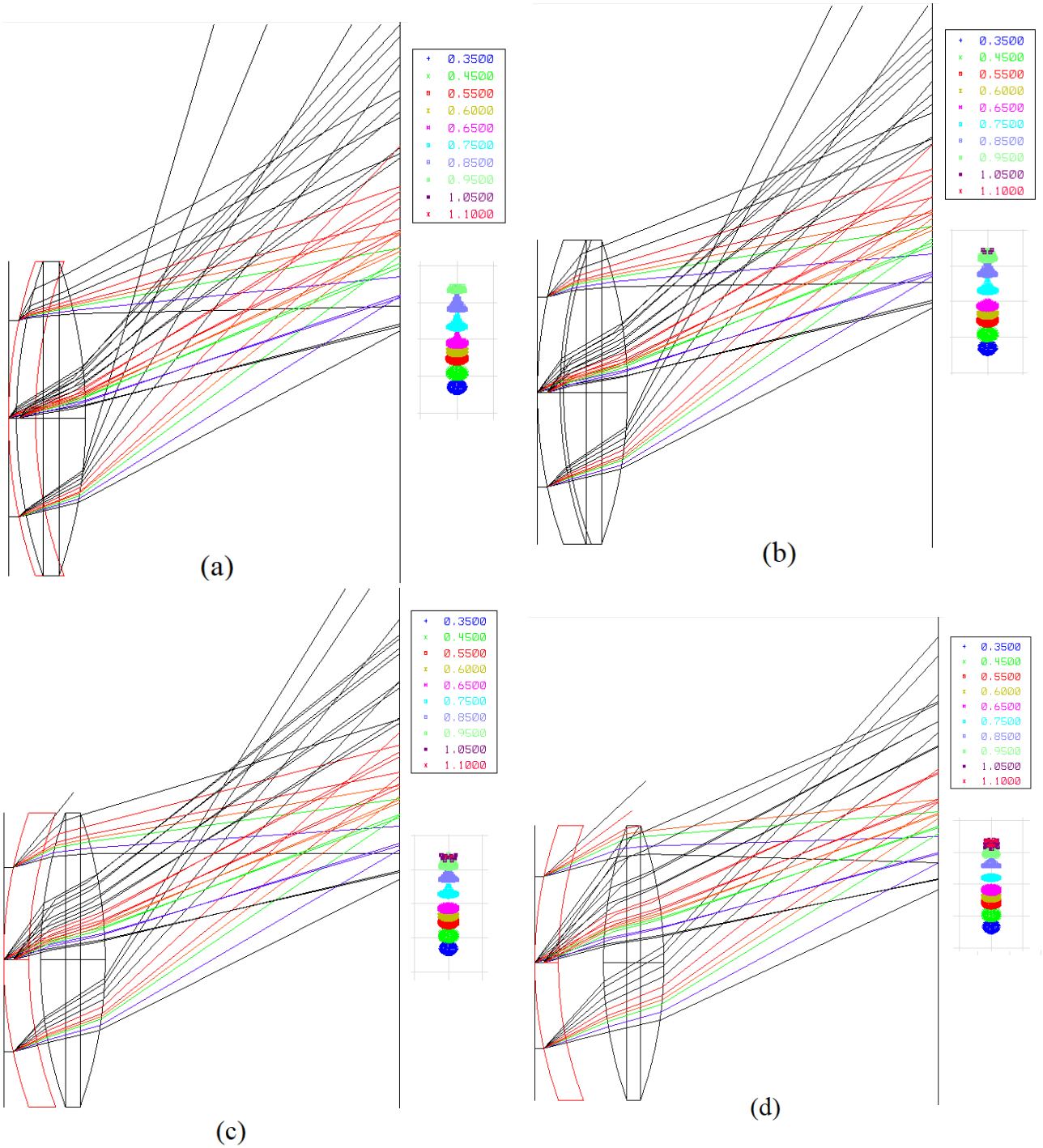

Figure 4 Four configurations according to lens-grating distance. (a) 1mm (b) 3mm (c) 5mm (d) 10mm

If the two elements were too close, it was observed that some of the wavelengths encountered the lens at angles that were not focused enough. However, if the spacing was too large, some of the rays diffracted by the grating escaped the system in the air gap without passing through the lens. The distance of 3 mm was found to be the adequate balance between a compact design and yielded performance at the fixed values of the rest of design variables. Considering the spot diagrams for each configuration, the difference in spectral separation for the band of interest was negligible for our application, though the off-axis distances and foci were being affected.

The primary performance metric chosen to judge the design methodology was the photocurrent, which was compared to the photocurrent from the individual cells covering the entire area. The photocurrent (or more accurately, photocurrent density), J_L was calculated from a given spectrum and external quantum efficiency using the following equation [30],

$$J_L = -q.\int E(\lambda).\frac{\lambda}{h.c}.EQE(\lambda)d\lambda \tag{6}$$

As the EQE data available for both receivers and the irradiance was with a resolution of 1 nm and the irradiance data in the ASTM G-173 standard was in $Wm^{-2}.nm^{-1}$, the integral equation was simplified into the following discrete summation,

$$J_L = \sum E(\lambda).\frac{\lambda}{h.c}.EQE(\lambda) \tag{7}$$

Equation 4.2 was implemented in the numerical computing software GNU Octave and it was simulated for both PV receivers separately in their own wavelength ranges. For simulation, the ASTM G-173 data was loaded according to the range and resolution of the EQE data available (from 350 to 1100nm range, steps of 1nm, using the direct irradiance only. The EQE data was provided by Wisnu Anand and its measurement is detailed in [31]. The term $E(\lambda)$ in the above equation was furst calculated by considering the grating efficiency, attenuation due to lens material and the concentration due to the lens.

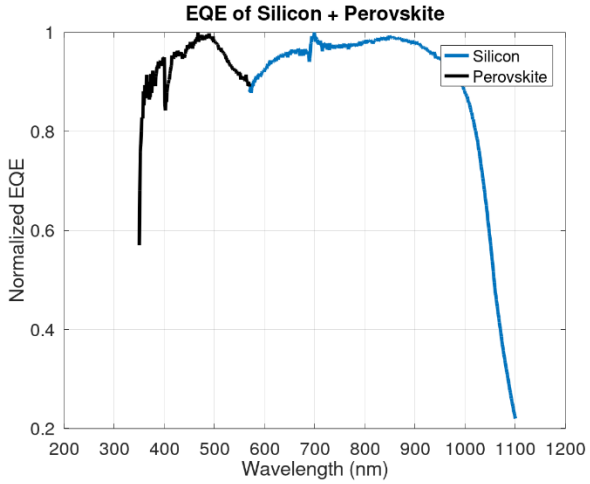

Figure 5 Combined EQE of Silicon and Perovskite used by the system

It was found that the photocurrent density was I_L = 84.999 $\frac{mA}{cm^2}$ for the designed system with Silicon and Perovskite double junction. For comparison, photocurrent calculated for Silicon without any of the optical manipulation, using the same data was I_{LSi0} = 32.625 $\frac{mA}{cm^2}$ and for Perovskite it was I_{LP0} = 18.768 $\frac{mA}{cm^2}$.

CONCLUSION

A two-junction, diffractive spectrum splitting system was designed and evaluated using simulations, in the light of literature, optics theory and available data. Its performance was judged primarily by calculating the photocurrent density and it showed great performance improvements when compared to the same PV cells without optical manipulation. The proposed design methodology could be particularly useful in prototyping spectrum splitting systems for checking various combinations of PV cells. The design and analysis methods used here could be further improved from various aspects such as taking into account particular grating surface profile type, considering the concentration ratios and grating spacing in the design process and temperature due to splitting and concentration, which can affect the photocurrent, but wasn't a part of the analysis. These could result in better designs that are more accurately characterized by the analysis method, before they manufactured or assembled.

//Not published at the time of printing of this thesis

REFERENCES

1. Stocker, T.F., D. Qin, G.-K. Plattner, M. Tignor, S.K. Allen, J. Boschung, A. Nauels, Y. Xia, V. Bex and P.M. Midgley (eds.) “IPCC, 2013: Climate Change 2013: The Physical Science Basis. Contribution of Working Group I to the Fifth Assessment Report of the Intergovernmental Panel on Climate Change”. Cambridge University Press, Cambridge, United Kingdom and New York, NY, USA, 1535 pp, 2013
2. Michael Schmela, “Report: Global Market Outlook 2018-2022", Solar Power Europe, 27th June 2018.
3. William Shockley, J. Hans Queisser, “Detailed Balance Limit of Efficiency of p-n Junction Solar Cells”, Journal of Applied Physics, Vol. 32, Issue 3, pp 510-519, 1961.
4. Sven Rühle, “Tabulated values of the Shockley–Queisser limit for single junction solar cells”, Solar Energy, Volume 130, pp 139-147, 2016.
5. MA Green, Y Hishikawa, ED Dunlop, Dean H. Levi, Jochen Hohl-Ebinger, Masahiro Yoshita, Anita W.Y. Ho-Baillie, “Solar cell efficiency tables (Version 53)”, Progress in Photovoltaics: Research and Applications, Vol. 27, Issue 1, pp 3-12, 2019.
6. A.G. Imenes, D.R. Mills, “Spectral beam splitting technology for increased conversion efficiency in solar concentrating systems: a review,” Solar Energy Materials and Solar Cells, Volume 84, Issues 1–4, Pages 19-69, 2004.
7. P. Blain, C. Michel, L. Clermont, F. Languy, M. Décultot, S. Habraken, C. Lenaerts, K. Fleury-Frenette, D. Vandormael and J. Loicq, “Spectral splitting planar solar concentrator: Experimental testing of a design aiming at dye sensitized solar cells,” Proc. of SPIE Vol. 9140, Photonics for Solar Energy Systems V, 2014.
8. Silvana Ayala P., Shelby Vorndran, Yuechen Wu, Benjamin Chrysler, Raymond Kostuk, “Segmented Holographic Spectrum Splitting Concentrator,” Next Generation Technologies for Solar Energy Conversion VII, Proc. of SPIE Vol. 9937, 2016.
9. Céline Michel, Jérôme Loicq, Tanguy Thibert, and Serge Habraken, “Optical study of a spectrum splitting solar concentrator based on a combination of a diffraction grating and a Fresnel lens,” AIP Conference Proceedings 1679, 070002, 2015.
10. Ahmad Mojiri, Robert Taylor, Elizabeth Thomsen, Gary Rosengarten, “Spectral beam splitting for efficient conversion of solar energy—A review”, Renewable and Sustainable Energy Reviews, Volume 28, Pages 654-663, 2013.
11. Hisashi Uzu, Mitsuru Ichikawa, Masashi Hino, Kunihiro Nakano, Tomomi Meguro, José Luis Hernández, Hui-Seon Kim, Nam-Gyu Park, and Kenji Yamamoto, “High efficiency solar cells combining a perovskite and a silicon heterojunction solar cells via an optical splitting system,” Applied Physics Letters 106, 013506, 2015.
12. Carlo Maragliano, Matteo Chiesa and Marco Stefancich, “Point-focus spectral splitting solar concentrator for multiple cells concentrating photovoltaic system,” Journal of Optics, Volume 17, 105901, Number 10, 2015.
13. Carlo Maragliano, Harry Apostoleris, Matteo Bronzoni, Stefano Rampino, Marco Stefancich, and Matteo Chiesa, "Efficiency enhancement in two-cell CIGS photovoltaic system with low-cost optical spectral splitter," Opt. Express 24, A222-A233, 2016.
14. Kaifeng Wu, Hongbo Li, Victor I. Klimov, “Tandem luminescent solar concentrators based on engineered quantum dots”, Nature Photonics, Volume 12, Issue 2, p.105-110, 2018
15. Francesco Meinardi, Samantha Ehrenberg, Lorena Dhamo, Francesco Carulli, Michele Mauri, Francesco Bruni, Roberto Simonutti, Uwe Kortshagen and Sergio Brovelli, “Highly efficient luminescent solar concentrators based on earth-abundant indirect-bandgap silicon quantum dots” Nature Photonics, Volume 11, Issue 3, 177-185, 2017.
16. Yuechen Wu, Benjamin D. Chrysler, Raymond K. Kostuk, "Design and fabrication of cascaded dichromate gelatin holographic filters for spectrum-splitting PV systems," Journal of Photonics for Energy 8(1), 017001, 2018.
17. Yuechen Wu, Raymond K. Kostuk, "Two-junction holographic spectrum-splitting micro-concentrating photovoltaic system," Journal of Photonics for Energy, SPIE, Vol. 7, 017001, 2017.
18. Jia Li, Wen-Qi Xu, Jia-Sheng Ye, Peng Han, Wen-Feng Sun, Sheng-Fei Feng, Xin-Ke Wang, Yan Zhang, “High focusing efficiency or high signal-to-noise ratio diffractive optical element for color separation and light focusing,” Optik, Volume 138, Pages 87-94, 2017.
19. Benjamin D. Chrysler, Yuechen Wu, Zhengshan Yu, Raymond K. Kostuk, “Volume holographic lens spectrum-splitting photovoltaic system for high energy yield with direct and diffuse solar illumination,” Next Generation Technologies for Solar Energy Conversion VIII, Proceedings of SPIE Vol. 10368, 103680G, 2017.

20. Céline Michel, Pascal Blain, Lionel Clermont, Fabian Languy, Cédric Lenaerts, Karl Fleury-Frenette, Marc Décultot, Serge Habraken, Denis Vandormael, Rudi Cloots, Gopala Krishna V.V. Thalluri, Catherine Henrist, Pierre Colson, Jérôme Loicq, “Waveguide solar concentrator design with spectrally separated light”, Solar Energy, Volume 157, Pages 1005-1016, 2017.
21. Cameron Stanley, Ahmad Mojiri and Gary Rosengarten, "Spectral light management for solar energy conversion systems," Nanophotonics, Vol. 5, Issue 1, Pages 161-179, 2016.
22. Abbas Albarazanchi, Philippe Gérard, Pierre Ambs, Patrick Meyrueis, Giang-Nam Nguyen, and Kevin Heggarty, "Smart multifunction diffractive lens experimental validation for future PV cell applications," Optics Express, 24, A139-A145, 2016.
23. Celine Michel, Jerome Loicq, Tanguy Thibert, Serge Habraken, "Optical Study of diffraction grating/Fresnel lens combinations applied to a spectral-splitting solar concentrator for space applications", Applied Optics, Vol. 54, No. 22, Pages 6666-6673, 2015.
24. Celine Michel, Jerome Loicq, Fabian Languy, Serge Harbraken, "Optical study of a solar concentrator for space applications based on a diffractive/refractive optical combination", Solar Energy Materials and Solar Cells, Volume 120, Part A, Pages 183-190, 2014.
25. Wen-Qi Xu, Dong-Feng Lin, Xin Xu, Jia-Sheng Ye, Xin-Ke Wang, Sheng-Fei Feng, Wen-Feng Sun, Peng Han, Yan Zhang, Qing-Bo Meng and Guo-Zhen Yang, “Simple and universal method in designs of high-efficiency diffractive optical elements for spectrum separation and beam concentration”, Chinese Phys. B Vol 26, No. 7, 074202, 2017.
26. Benjamin Chrysler, Silvana Ayala Pelaez, Yuechen Wu, Shelby Vorndran, Raymond Kostuk, “Environmental stability study of holographic solar spectrum splitting materials,” Next Generation Technologies for Solar Energy Conversion VII, Proc. of SPIE Vol. 9937, 2016.
27. Francis Jenkins, Harvey White, “Fundamentals of Optics,” 4th Ed. McGraw-Hill.
28. Juan M. Russo, Shelby Vorndran, Yuechen Wu, Raymond Kostuk, "Comparison of Dispersive and Non-Dispersive Spectrum Splitting Techniques for Photovoltaic Systems", IEEE 40th Photovoltaic Specialist Conference (PVSC), Denver, CO, pp. 2257-2261, 2014.
29. Alexander Scheeline, “How to Design a Spectrometer.” *Applied Spectroscopy*, Vol. 71, No. 10, 2237–52 (October 2017).
30. K. Jager, O. Isabella, R. van Swaaij, A. H.M. Smets, and M. Zaman, *Solar Energy - Fundamentals, Technology, and Systems*. Delft University of Technology, 2014.
31. W. Ananda, “External quantum efficiency measurement of solar cell,” in *2017 15th International Conference on Quality in Research (QiR) : International Symposium on Electrical and Computer Engineering*, Nusa Dua, 2017, pp. 450–456.